remote sensing

MDPI

Article

Machine Learning-Based Mapping of Dominant Tree Species in Dryland Forests Using Multi-Temporal and Multi-Source Data

Emad H. E. Yasin [1,2,*], Milan Koreň [3] and Kornel Czimber [1]

[1] Institute of Geomatics and Civil Engineering, Faculty of Forestry, University of Sopron, Bajcsy-Zsilinszky u. 4., 9400 Sopron, Hungary; czimber.kornel@uni-sopron.hu
[2] Department of Forest Management, Faculty of Forestry, University of Khartoum, Khartoum North 13314, Sudan
[3] Department of Forest Resource Planning and Informatics, Faculty of Forestry, Technical University in Zvolen, T. G. Masaryka 24, 960 01 Zvolen, Slovakia; milan.koren@tuzvo.sk
* Correspondence: emad.hassanelawadyasin@phd.uni-sopron.hu or emad.yasin@uofk.edu

Highlights

What are the main findings?

- Multi-temporal and multi-sensor machine learning in GEE achieved high classification accuracy (OA up to 96%, κ up to 93%).
- RF and SVM consistently outperformed CART and the ensemble model.
- Sentinel-2 improved species discrimination due to higher spatial and spectral resolution.
- Classification separability declined over time (decreasing MCC), indicating increasing ecological complexity.
- Species composition shifted, with a decline in *Acacia seyal* and an increase in *Sterculia setigera*.

What are the implications of the main findings?

- The framework provides a scalable and cost-effective solution for long-term dryland forest monitoring.
- Species-level mapping improves detection of ecological change under anthropogenic and climatic pressures.

Abstract

Timely and accurate mapping of tree species is essential for forest resource inventory, biodiversity conservation, and sustainable ecosystem management, particularly in dryland environments where structural heterogeneity, spectral similarity, and data scarcity complicate classification. This study develops a machine learning-based framework implemented in Google Earth Engine to map dominant tree species in the Elnour Natural Forest Reserve (ENFR), Blue Nile, Sudan, using multi-temporal and multi-sensor remote sensing data. Multi-temporal Landsat 5 TM, Landsat 8 OLI, and Sentinel-2 MSI imagery were integrated with vegetation index (NDVI), topographic variables derived from a digital elevation model (DEM), and field observations. The performance of Random Forest (RF), Support Vector Machine (SVM), Classification and Regression Trees (CART), and an unweighted ensemble approach was evaluated across four reference years (2008, 2013, 2018, and 2021). Results show that RF and SVM consistently achieved high classification performance, with overall accuracy (OA) ranging from 85.0% to 92.0% and Kappa

Academic Editors: Jia Wang, Brenden E. McNeil, Fang Huang, Lingling Ma and Peng Liu

Received: 26 February 2026
Revised: 4 April 2026
Accepted: 11 April 2026
Published: 15 April 2026

Copyright: © 2026 by the authors. Licensee MDPI, Basel, Switzerland. This article is an open access article distributed under the terms and conditions of the Creative Commons Attribution (CC BY) license.

coefficients (κ) from 0.81 to 0.89, while maintaining stable and ecologically realistic species-area estimates. CART showed greater sensitivity to class imbalance and overestimated minor species (OA = 72.0–80.0%, κ = 0.65–0.74), whereas the ensemble approach amplified misclassification of rare classes (OA = 78.0–84.0%, κ = 0.70–0.78). The integration of Sentinel-2 data improved species discrimination due to enhanced spatial and spectral resolution, particularly in the red-edge region; however, algorithm selection remained the dominant factor controlling performance. Feature importance analysis identified near-infrared (NIR), shortwave infrared (SWIR), and NDVI variables as the most influential predictors. Multi-temporal analysis revealed declining class separability, reflected by decreasing MCC values, and a shift in species composition, including a decline in *Acacia seyal* (Delile) and an increase in *Sterculia setigera* Delile. These patterns indicate increasing ecological complexity driven primarily by anthropogenic pressures, with climatic variability acting as an additional stressor.

Keywords: dryland forests; tree species mapping; machine learning; Random Forest; Support Vector Machine; Classification and Regression Trees; multi-temporal satellite data; Google Earth Engine; remote sensing; species classification

1. Introduction

Dryland ecosystems, particularly in Sudan, provide essential ecological and socio-economic services, supporting millions of people through food, fuelwood, and ecosystem functions [1–5]. These ecosystems, which cover approximately 30% of Sudan's land area [6], are increasingly threatened by a combination of anthropogenic pressures, including deforestation, urbanization, overgrazing, and land use conversion, and natural stressors such as soil erosion, desertification, and climate change [7–9]. Climatic projections further indicate that savanna woodlands and dryland forests in Sudan will experience accelerated warming and drying trends, leading to increased ecosystem degradation and altered vegetation structure [8,10,11].

Forests play a crucial role in maintaining ecological balance, supporting food security, and sustaining biodiversity [11–16]. In Blue Nile State, for example, natural forest reserves and riverine ecosystems support high levels of plant and animal diversity and underpin key ecological processes [11,17]. Trees and shrubs in Sudanese drylands are particularly important for combating desertification and supporting rural livelihoods, especially through indigenous fruit trees and agroforestry systems, which can contribute up to 50% of household income [14,18,19]. These ecological and socio-economic roles highlight the importance of understanding forest composition and dynamics under increasing environmental and anthropogenic pressures.

Accurate mapping and monitoring of forest composition, particularly dominant tree species, are critical for sustainable forest management, biomass estimation, and ecosystem modeling [20,21]. Tree species-level information supports ecological assessments, carbon stock estimation, and habitat management. However, conventional field-based forest inventories are often constrained by high costs, labor intensity, and limited spatial coverage, making them insufficient for large-scale or long-term monitoring, particularly in remote and environmentally sensitive regions [20,22].

Despite advances in remote sensing, tree species classification in dryland ecosystems remains technically challenging [23]. Dryland forests are characterized by sparse and discontinuous vegetation, heterogeneous canopy structures, and strong seasonal variability in spectral responses [24,25]. These characteristics lead to high spectral similarity among

species, increased intra-class variability, and reduced separability between vegetation types when using conventional classification methods [26,27].

In addition, the dominance of a few species alongside many rare or sparsely distributed taxa introduces class imbalance, which can bias classification models toward dominant species and reduce accuracy for minor classes. Medium-resolution imagery (10–30 m), although widely available, may further limit the detection of fine-scale canopy heterogeneity, increasing spectral confusion among structurally similar species. Consequently, traditional approaches often underestimate species diversity and spatial extent, particularly in complex dryland environments [26,27]. These limitations underscore the need for advanced methodologies capable of integrating multiple data sources and addressing the inherent complexity of dryland ecosystems [28].

Satellite remote sensing provides practical, scalable, and repeatable observations for forest monitoring [12]. Medium-resolution imagery from Landsat 5 TM, Landsat 8 OLI, and Sentinel-2 offers long-term, freely available datasets suitable for regional-scale analyses [20,29–31]. The integration of spectral bands with vegetation indices, such as the Normalized Difference Vegetation Index (NDVI), and topographic variables derived from Digital Elevation Models (DEM) enhances tree species discrimination by capturing vegetation vigor, moisture conditions, and environmental gradients [26,27,31,32]. Field observations remain essential for calibration and validation, providing ground truth data to improve classification reliability [22,33].

However, single-date or single-source imagery often fails to capture the temporal variability of vegetation in dryland environments, where phenological changes strongly influence spectral responses [24,25,34]. Multi-temporal and multi-source datasets enable the integration of complementary information, improving classification accuracy and robustness by capturing seasonal dynamics and structural variability [26,28,35]. Machine learning algorithms, including Random Forest (RF), Support Vector Machine (SVM), Classification and Regression Trees (CART), and ensemble approaches, are well-suited for processing such high-dimensional and heterogeneous datasets [28]. RF and CART are non-parametric and capable of modeling complex interactions between predictor variables, while SVM is effective in separating classes in high-dimensional feature spaces, particularly under conditions of spectral overlap [26,27,36–38]. Ensemble approaches aim to combine the strengths of individual classifiers; however, their effectiveness depends on the diversity and complementarity of the models, and simple aggregation strategies may not always improve performance in class-imbalanced and spectrally complex environments [28].

Cloud-based platforms such as Google Earth Engine (GEE) provide an unprecedented opportunity to process and analyze large volumes of remote sensing data efficiently [28,39,40]. GEE enables access to multi-temporal satellite archives and offers powerful computational capabilities for implementing machine learning models at regional scales without the limitations of local processing resources. It also supports reproducible workflows and rapid testing of multiple data-model configurations, which is particularly valuable for heterogeneous and data-scarce dryland environments [28,41].

Despite these advances, a critical gap remains in developing robust and scalable frameworks for long-term, species-level mapping in dryland forests that effectively integrate multi-temporal and multi-source data while addressing challenges such as spectral similarity, class imbalance, and data scarcity. Many existing studies are limited to single sensors, short time periods, or a restricted number of species, reducing their applicability for long-term ecological monitoring and management.

Therefore, this study develops a machine learning-based framework fully implemented in GEE to map dominant tree species in Sudanese dryland forests using Landsat 5, Landsat 8 OLI, Sentinel-2, NDVI, DEM, and field observations. The specific objectives

are to: (1) evaluate the performance of RF, SVM, CART, and ensemble models for tree species classification across multiple time periods (2008, 2013, 2018, and 2021); (2) identify the optimal combinations of datasets and algorithms for dryland forest mapping; and (3) analyze spatiotemporal changes in dominant tree species distribution within the Elnour Natural Forest Reserve (ENFR). By addressing key methodological and ecological challenges, this study provides a reproducible and scalable framework for monitoring dryland forest dynamics and supports sustainable forest management and biodiversity conservation under changing environmental conditions.

2. Materials and Methods

2.1. Study Area

This study was conducted in the Blue Nile region of southeastern Sudan within the Elnour Natural Forest Reserve (ENFR), located between 11°48′19″–11°53′30″N and 34°28′47″–34°32′35″E, approximately 6 km southeast of El Damazin and 3 km east of El Rosaries. The reserve was officially designated on 15 June 1959 and covers an area of 4667.17 ha, providing legal protection for biodiversity conservation and reducing pressures such as illegal logging and hunting (Figure 1). Although spatially limited, ENFR represents a typical dryland woodland ecosystem in Sudan and serves as a suitable case study for evaluating machine learning-based species classification in heterogeneous and data-scarce environments.

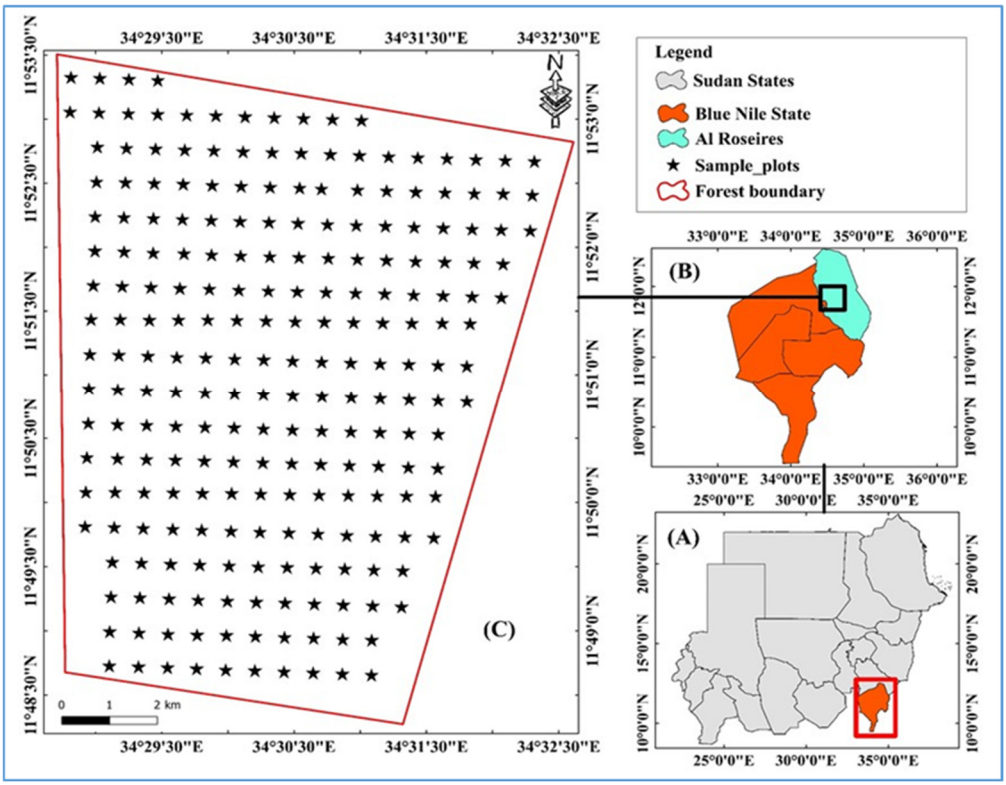

Figure 1. Maps for the location of Blue Nile State in southeastern Sudan (**A**) and the location of Elnour Natural Forest Reserve (study area) in Blue Nile State (**B**), as well as the overview of Elnour Natural Forest Reserve (**C**).

The climate of the region is tropical subcontinental, characterized by a distinct wet season (June–October) and dry season (November–May). Mean temperatures range from approximately 15.6–16.4 °C during the coolest months (December–January) to 39.9–41.5 °C during the hottest period (April–May). Annual rainfall varies between 300 and 700 mm, with a peak between July and September, primarily influenced by South Atlantic and

Congo air masses, with limited contribution from the Indian Ocean. This pronounced seasonal variability strongly influences vegetation phenology and spectral response, posing challenges for remote sensing-based species discrimination.

According to the vegetation classification of Harrison and Jackson [42], ENFR is categorized as low-rainfall woodland savannah and supports approximately 55 woody species from 36 genera and 18 families [43]. Dominant species in the reserve include *Sterculia setigera* Delile, *Combretum hartmannianum* Schweinf., *Acacia seyal* (Delile), *Terminalia brownii* Fresen., *Terminalia laxiflora* Engl., *Anogeissus leiocarpus* (DC.) Guill. & Perr., *Balanites aegyptiaca* (L.) Delile, *Combretum micranthum* G.Don, and *Lannea fruticosa* (Hochst. ex A.Rich.) Engl. [44]. The reserve also contains ecologically important and threatened species such as *Adansonia digitata* L., *Boswellia papyrifera* (Delile) Hochst., *Dalbergia melanoxylon* Guill. & Perr., *Grewia* spp., *Lonchocarpus laxiflorus* Guill. & Perr., *Piliostigma reticulatum* (DC.) Hochst., and *Xeromphis nilotica* (Stapf) Keay [45]. This diversity, combined with the dominance of a few species and the presence of many rare taxa, creates a class-imbalanced system that complicates classification tasks.

Topographically, ENFR is relatively flat with localized depressions, particularly in central and northern clay-rich areas [46]. Soils are dominated by dark cracking clays (64.2%) and sandy loam to gravelly soils (35.8%), influencing vegetation distribution and productivity. Human activities also play a significant role in shaping forest structure. Local communities from El Azaza village and surrounding areas depend on the forest for fuelwood, grazing, and non-timber forest products, particularly during the dry season (March–May). These anthropogenic pressures, combined with climatic variability, contribute to spatial and temporal changes in species composition, making ENFR a representative system for studying dryland forest dynamics using remote sensing and machine learning approaches.

2.2. Data Collection and Analysis

This study employs a structured and reproducible workflow to map dominant tree species by integrating remote sensing data, field observations, and machine learning techniques (Figure 2). Multi-temporal datasets for 2008, 2013, 2018, and 2021 were used to capture long-term changes in forest composition under varying environmental and anthropogenic conditions. This framework ensures consistent data processing, reliable classification, and robust analysis of species distribution dynamics.

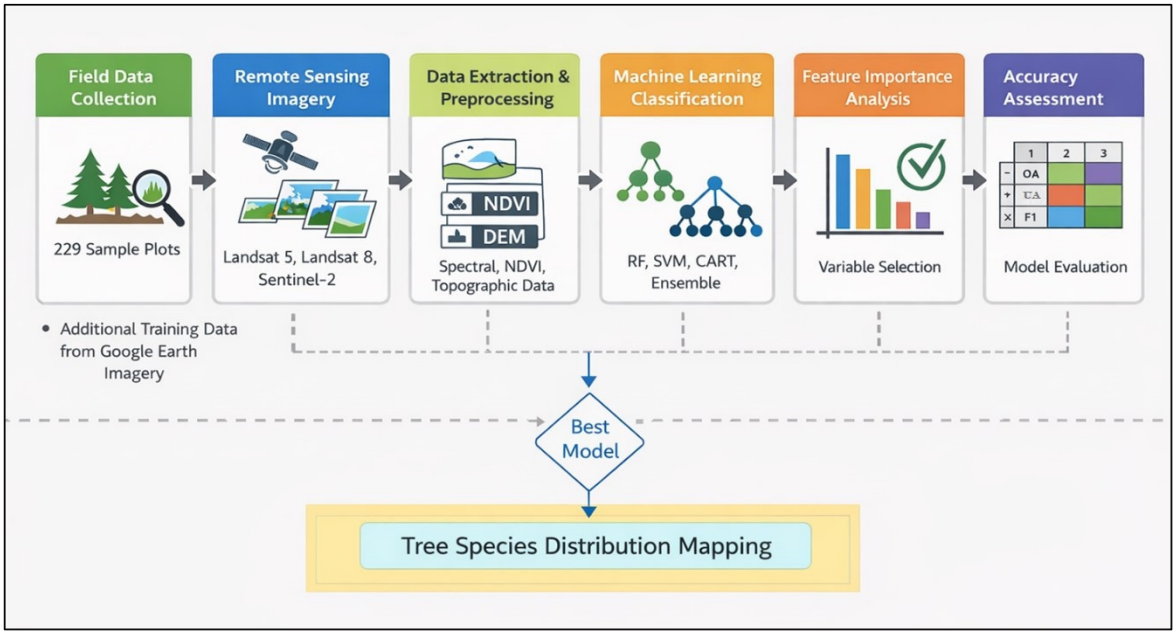

Figure 2. Workflow of the study showing field data collection, multi-source remote sensing data, feature extraction, machine learning classification (RF, SVM, CART, ensemble), feature importance analysis, and accuracy assessment. Accuracy is evaluated using confusion matrix metrics (OA, UA, and F1), where colors indicate classification performance. Solid arrows represent processing steps, and dashed arrows indicate model refinement leading to the best model for tree species distribution mapping..

2.2.1. Remote Sensing Data Collection and Processing

Multi-temporal satellite imagery was used to ensure consistent medium-resolution coverage of the study area. Landsat 5 TM imagery was used for 2008, Landsat 8 OLI for 2013 (post-launch period), and Sentinel-2 MSI for 2018 and 2021. All images were selected from the dry season (October–March) to minimize cloud contamination and reduce phenological variability in vegetation reflectance [18,47].

All preprocessing steps were performed in Google Earth Engine (GEE) to ensure consistency across sensors. The processing workflow included cloud masking using quality assessment bands, removal of low-quality pixels, and radiometric normalization [39,40]. Vegetation indices, particularly the Normalized Difference Vegetation Index (NDVI), were calculated to enhance vegetation signal separability. To further reduce noise and represent peak vegetation conditions, NDVI-based greenest-pixel composites were generated using quality mosaicking, whereby the highest NDVI value was selected for each pixel [25,36,48].

For each year, predictor variables were organized into multi-layer image stacks (hereafter referred to as "image cubes"), consisting of spectral bands, derived vegetation indices, and topographic variables. Spatial resolution was standardized to 30 m for Landsat-based years and 10–20 m for Sentinel-2, with resampling applied where necessary to ensure consistency. Each image cube included multiple temporal observations within the selected season, enabling representation of phenological variability. Topographic variables, including elevation, slope, and aspect, were derived from a DEM (SRTM) using standard terrain functions available in GEE. These variables capture environmental gradients influencing species distribution [22,32,34]. The integration of multi-source datasets improves classification robustness by combining spectral, structural, and environmental information [20,26,49].

2.2.2. Training Samples Collection and Dataset Preparation

A total of 229 permanent sample plots (radius = 17.84 m; area = 1000 m^2) were established to provide reliable ground reference data. The plots were systematically designed using a stratified approach to capture variability in species composition, soil types, and topographic conditions across the study area. These permanent plots were initially established in 2008 and consistently revisited in subsequent years (2013, 2018, and 2021) to monitor temporal changes in vegetation structure and species composition. Within each plot, all woody species were identified by a trained botanist to ensure taxonomic accuracy and consistency [50,51].

To enhance spatial representativeness and address limitations associated with field accessibility, additional training samples were derived from high-resolution Google Earth imagery, particularly in areas that were difficult to access [20,52]. A stratified sampling strategy was applied to ensure proportional representation of dominant and secondary species. However, due to the inherent ecological structure of dryland forests, where a few dominant species prevail and many species occur sparsely, class imbalance remained unavoidable.

To mitigate the effects of class imbalance, several measures were implemented: (i) enforcing minimum sample thresholds for minority classes through stratified sampling,

(ii) careful selection and validation of training polygons to avoid misclassification, and (iii) evaluating model robustness across multiple classifiers (RF, SVM, and CART), which differ in their sensitivity to imbalanced data. These steps improved classification stability and reduced bias toward dominant classes.

Missing or inconsistent samples in Google Earth Engine (GEE), resulting from cloud contamination, sensor noise, or spatial misalignment, were identified and removed using strict quality control criteria. Replacement samples were then selected based on temporal consistency across years, visual verification using high-resolution imagery, and agreement with field observations. Only samples with clear spectral signatures, accurate spatial alignment, and consistent class labeling were retained, thereby minimizing noise in the training dataset.

For each reference year, the dataset was divided into 70% for model training and 30% for independent validation. In addition, stratified 5-fold cross-validation was applied during hyperparameter tuning to ensure robust and unbiased model evaluation. Predictor variables, including spectral bands, vegetation indices (e.g., NDVI), and DEM-derived features (elevation, slope, and aspect), were extracted for each sample, forming standardized multi-source feature datasets for classification [36,53].

2.2.3. Variable Selection and Feature Importance

Accurate classification of tree species in dryland environments depends on the selection of predictor variables that effectively capture spectral, structural, and environmental variability. In this study, predictor variables were systematically selected based on their ecological relevance and proven effectiveness in vegetation mapping. The final feature set included multi-temporal spectral bands from Landsat (TM, OLI) and Sentinel-2 (MSI), vegetation indices (primarily NDVI and its temporal derivatives), and topographic variables derived from a Digital Elevation Model (DEM), including elevation, slope, and aspect.

Spectral bands in the red, near-infrared (NIR), and shortwave infrared (SWIR) regions were selected due to their sensitivity to vegetation structure, chlorophyll content, and canopy moisture conditions. NDVI was included to capture vegetation vigor and phenological dynamics, which are critical for distinguishing species with similar structural characteristics but different seasonal responses in dryland forests [25,26,34]. Topographic variables were derived from the Shuttle Radar Topography Mission (SRTM) DEM using standard terrain analysis functions in Google Earth Engine, where slope and aspect were calculated from elevation gradients. These variables were incorporated to account for environmental controls on species distribution, particularly soil moisture availability and micro-topographic variation.

Feature importance was evaluated separately for each classifier to reflect the different learning mechanisms. For Random Forest (RF), permutation-based importance was used to quantify the contribution of each variable to classification accuracy [54]. For CART, importance was derived from split frequency and node hierarchy within the decision tree [55], while for Support Vector Machine (SVM), sensitivity analysis was applied to assess the influence of input variables on model outputs [56,57]. An ensemble approach aggregated 224 importance rankings across classifiers, improving robustness and predictive stability [58–60].

To address the methodological limitation of directly comparing importance metrics across classifiers with different mathematical foundations, variable importance values were normalized and ranked within each model before cross-model comparison. An aggregated ranking approach was then applied to identify consistently important variables across classifiers and years, rather than directly comparing absolute importance values.

This approach improves interpretability while maintaining methodological consistency, although it does not fully eliminate differences in how importance is quantified.

In addition, the theoretical framework of Shapley Additive Explanations (SHAP) was considered to provide a model-agnostic interpretation of feature contributions. SHAP quantifies the marginal contribution of each feature to the model prediction based on cooperative game theory [61]. The SHAP value for feature i is defined as

$$\phi_i = \sum_{S \subseteq F \setminus \{i\}} \frac{|S|!(|F|-|S|-1)!}{|F|!} \left[f_{S\cup\{i\}}(x_{S\cup\{i\}}) - f_S(x_S) \right] \quad (1)$$

where F represents the full set of input features, S is a subset of features excluding feature i, and ϕ_i represents the marginal contribution of feature $i$averaged over all possible feature subsets. The model prediction can be expressed as an additive combination of feature contributions:

$$f(x) = \phi_0 + \sum_{i=1}^{M} \phi_i \quad (2)$$

where ϕ_0 is the expected model output and M is the total number of features. For global interpretation, feature importance can be summarized using the mean absolute SHAP value across all samples.

However, due to computational and platform limitations within Google Earth Engine (GEE), full SHAP implementation was not feasible in this study. Therefore, feature importance was assessed using classifier-specific importance measures and a normalized aggregation approach, which ensures consistent and interpretable comparison across models.

The consistent application of this framework across all study years (2008, 2013, 2018, and 2021) ensured that temporal variations in feature importance reflect genuine ecological changes rather than differences in model structure or variable selection procedures [28]. All predictor variables used in this study, including their definitions, spectral characteristics, and data sources, are summarized in Table 1 to ensure transparency and reproducibility of the classification framework.

Table 1. Predictor Variables Used for Tree Species Classification.

Category	Variable	Description	Sensor/Source	Ecological Relevance
Spectral Bands	Blue (B2/SR_B2)	Visible blue reflectance	Landsat/Sentinel-2	Sensitive to atmospheric effects and soil background
Spectral Bands	Green (B3/SR_B3)	Visible green reflectance	Landsat/Sentinel-2	Related to vegetation greenness
Spectral Bands	Red (B4/SR_B4)	Chlorophyll absorption region	Landsat/Sentinel-2	Key for vegetation discrimination
Spectral Bands	NIR (B5/B8)	Near-infrared reflectance	Landsat/Sentinel-2	Sensitive to canopy structure and biomass
Spectral Bands	SWIR1 (B6/B11)	Shortwave infrared	Landsat/Sentinel-2	Moisture content and vegetation stress
Spectral Bands	SWIR2 (B7/B12)	Shortwave infrared	Landsat/Sentinel-2	Soil–vegetation moisture interaction
Vegetation Index	NDVI	(NIR − Red)/(NIR + Red)	Derived	Vegetation vigor and productivity
Vegetation Index	Multi-temporal NDVI	NDVI across time periods	Derived	Captures phenological variability

Topographic	Elevation	Surface height above sea level	SRTM DEM	Controls temperature and moisture gradients
Topographic	Slope	Rate of elevation change	Derived from DEM	Influences runoff and soil moisture
Topographic	Aspect	Direction of slope	Derived from DEM	Affects solar radiation and microclimate

2.2.4. Machine Learning Algorithms

Supervised classification was implemented in Google Earth Engine (GEE) using three widely adopted machine learning algorithms representing different learning paradigms: Random Forest (RF), Support Vector Machine (SVM), and Classification and Regression Trees (CART). These algorithms were selected due to their proven effectiveness in handling high-dimensional, non-linear, and heterogeneous remote sensing data, particularly in dryland environments [20,26,36].

RF is an ensemble tree-based method that constructs multiple decision trees using bootstrap sampling and random feature selection, with final predictions derived through majority voting [54,62]. This approach reduces overfitting and improves generalization in complex datasets [63]. SVM is a margin-based classifier that identifies optimal separating hyperplanes in high-dimensional feature space; for non-linear classification, kernel functions are used to transform the data [56,64]. In this study, the radial basis function (RBF) kernel was adopted due to its strong performance in vegetation classification tasks [60]. CART is a non-parametric, single decision-tree model that partitions the feature space into homogeneous subsets based on impurity criteria, offering interpretability but higher sensitivity to noise and class imbalance [54].

An ensemble classification approach was additionally implemented to evaluate whether combining classifiers improves predictive performance. A hard-voting strategy was adopted, whereby each classifier (RF, SVM, and CART) produces a discrete class label, and the final class assignment is determined by majority agreement [65]. In cases where all classifiers predicted different classes (tie condition), the class with the highest confidence from the RF model was selected, given its generally robust performance. The inclusion of CART alongside RF and SVM was intended to introduce structural diversity into the ensemble by combining tree-based and margin-based learning approaches. However, the ensemble was treated as a comparative framework rather than a primary model to assess whether simple aggregation improves classification accuracy and robustness in dryland environments [65].

Since classifier performance is strongly influenced by hyperparameter selection, optimization was conducted independently for each model prior to ensemble construction [65]. Model optimization was performed using grid search, which systematically evaluates combinations of predefined parameter values to identify the configuration yielding the highest classification accuracy [66]. This process was integrated with stratified 5-fold cross-validation to ensure robust performance evaluation and reduce overfitting, particularly under class imbalance conditions.

2.2.5. Accuracy Assessment and Error-Adjusted Area Estimation

Classification performance was evaluated using a confusion matrix, which compares predicted and reference labels to quantify classification accuracy. From the confusion matrix, standard evaluation metrics were derived, including Overall Accuracy (OA), Producer's Accuracy (PA), User's Accuracy (UA), Kappa coefficient (κ), and F1-score [48,67–69].

Overall Accuracy (OA) represents the proportion of correctly classified samples relative to the total number of validation samples. Producer's Accuracy (PA) measures the probability that a reference sample is correctly classified and is therefore associated with

omission error. User's Accuracy (UA) represents the reliability of the classified map and is associated with commission error. The Kappa coefficient (κ) evaluates the agreement between predicted and reference classifications beyond chance. The F1-score provides a harmonic balance between precision and recall and is particularly suitable for evaluating classification performance under class imbalance conditions [48,68,69].

To ensure robust and unbiased evaluation, a two-stage validation strategy was applied. First, the dataset was divided into 70% for model training and 30% for independent validation. Second, stratified 5-fold cross-validation was implemented during hyperparameter tuning to assess model stability and generalization performance [57–59,67]. This combined approach ensures both independent validation and internal robustness of the models.

The accuracy assessment was conducted using the confusion matrix generated in Google Earth Engine (GEE) via the *errorMatrix* function, comparing reference and classified samples. The evaluation metrics were computed as follows:

$$OA = \frac{1}{N}\sum_{i=1}^{n} C_{ii} \tag{3}$$

$$PA_i = \frac{C_{ii}}{\sum_{j=1}^{n} C_{ij}} \tag{4}$$

$$UA_i = \frac{C_{ii}}{\sum_{j=1}^{n} C_{ji}} \tag{5}$$

$$F1_i = \frac{2 \cdot PA_i \cdot UA_i}{PA_i + UA_i} \tag{6}$$

$$\kappa = \frac{N\sum_{i=1}^{n} C_{ii} - \sum_{i=1}^{n}(R_i \cdot C_i)}{N^2 - \sum_{i=1}^{n}(R_i \cdot C_i)} \tag{7}$$

where n is the number of classes and N is the total number of observations. C_{ij} denotes the number of samples belonging to reference class i classified as class j, while C_{ii} represents correctly classified samples. R_i and C_i denote the row and column totals, respectively. The confusion matrix is structured such that rows correspond to reference classes and columns correspond to classified labels. Accordingly, PA_i reflects omission error, while UA_i reflects commission error.

In addition to conventional accuracy metrics, the Matthews Correlation Coefficient (MCC) was calculated to provide a more balanced evaluation of classification performance, particularly under multi-class and imbalanced conditions. MCC incorporates all elements of the confusion matrix and is less sensitive to class dominance compared to OA and Kappa, making it suitable for dryland ecosystems characterized by uneven class distributions. For multi-class classification, MCC was computed as

$$MCC = \frac{c \cdot s - \sum_k (p_k \cdot t_k)}{\sqrt{\left(s^2 - \sum_k p_k^2\right)\left(s^2 - \sum_k t_k^2\right)}} \tag{8}$$

where $c = \sum_k C_{kk}$ is the total number of correctly classified samples, $s = N$ is the total number of samples, p_k is the total number of samples predicted for class k, and t_k is the total number of reference samples for class k.

To improve the reliability of species-area estimation, error-adjusted area estimation was applied following best practices for accuracy assessment and area estimation in remote sensing [59,70–72]. Unlike direct map-based estimates, which may be biased due to

classification errors, this approach corrects area estimates using confusion matrix information.

The adjusted proportion of area for class i, denoted as $\hat{p}_i$, was calculated as

$$\hat{p}_i = \sum_{j=1}^{n} p_{ji} \cdot w_j \quad (9)$$

where p_{ji} is the proportion of reference samples in class j classified as class i, and w_j is the mapped area proportion of class j.

The corresponding error-adjusted area was then estimated as

$$\hat{A}_i = \hat{p}_i \times A \quad (10)$$

where $\hat{A}_i$ is the adjusted area of class i, and A is the total mapped area of the study region.

To quantify uncertainty, the variance of the estimated proportion was calculated as

$$\mathrm{Var}(\hat{p}_i) = \sum_{j=1}^{n} w_j^2 \cdot \frac{p_{ji}(1 - p_{ji})}{n_j - 1} \quad (11)$$

where n_j is the number of reference samples in mapped class j. The standard error was then derived as

$$SE(\hat{p}_i) = \sqrt{\mathrm{Var}(\hat{p}_i)} \quad (12)$$

Based on this, the 95% confidence limits (CL) were calculated as

$$CL_i = 1.96 \times SE(\hat{p}_i) \quad (13)$$

The final results were expressed as $\hat{p}_i \pm CL_i$ for proportional area and $\hat{A}_i \pm (CL_i \times A)$ for area estimates in hectares.

Overall, *OA*, *Kappa*, and *MCC* were used as primary indicators of classification performance, while class-level metrics (*PA*, *UA*, and *F*1-score) and error-adjusted area estimates were evaluated to ensure robust and unbiased interpretation of classification results across both dominant and less-represented species.

3. Results

3.1. Machine Learning-Based Classification of Dominant Tree Species

Machine learning classifiers were successfully applied to map dominant tree species across all reference years (2008, 2013, 2018, and 2021) using multi-temporal and multi-source satellite data processed within Google Earth Engine. All classifiers (RF, SVM, CART, and ensemble) were implemented using consistent training datasets, predictor variables, and preprocessing workflows, ensuring comparability across years.

The resulting classification maps revealed coherent and ecologically meaningful spatial patterns. *A. seyal* consistently dominated the landscape across all time periods, confirming its role as the primary canopy-forming species. Secondary species, including *S. setigera* and *C. hartmannianum*, were also consistently identified, although their spatial extent and distribution varied across years and classification algorithms.

In contrast, minor and sparsely distributed species exhibited higher classification uncertainty, particularly in areas of spectral overlap or mixed canopy conditions. This uncertainty was more pronounced in the ensemble outputs, reflecting the challenges of distinguishing rare species in dryland environments with heterogeneous vegetation structure and limited sample representation.

3.2. Classification Accuracy Assessment Across Algorithms and Years

Classification performance varied across algorithms and years, reflecting differences in model structure, sensor characteristics, and class separability. Model evaluation was based on Overall Accuracy (OA), Kappa coefficient (κ), Matthews Correlation Coefficient (MCC), and class-level metrics (Producer's Accuracy (PA), User's Accuracy (UA), and F1-score), with detailed results presented in Tables 2–6.

Table 2. Matthews Correlation Coefficient (MCC) values for RF, SVM, CART, and Ensemble classifiers across study years.

Year	RF	SVM	CART	Ensemble
2008	0.9148	0.9287	0.9288	0.8022
2013	0.8523	0.8736	0.8807	0.6772
2018	0.8318	0.8669	0.7411	0.5364
2021	0.8016	0.8389	0.8584	0.5197

Table 3. Accuracy Assessment of Machine Learning Classifiers (RF, SVM, CART, Ensemble) for Dominant Tree Species Identification in 2008.

Species	RF			SVM			CART			Ensemble		
	PA (%)	UA (%)	F1-Score	PA (%)	UA (%)	F1-Score	PA (%)	UA (%)	F1-Score	PA (%)	UA (%)	F1-Score
AS	98.68	96.33	97.00	98.94	97.00	98.00	98.94	96.85	98.00	97.19	91.37	94.00
CoH	89.29	92.21	91.00	92.31	93.00	93.00	90.73	94.38	93.00	68.34	83.1	75.00
SS	93.76	93.02	93.00	94.38	94.00	94.00	94.47	93.96	94.00	86.37	85.33	86.00
DC	75.86	100.00	86.00	80.33	100.00	89.00	79.37	100.00	89.00	52.38	94.29	67.00
ASe	82.91	96.04	89.00	88.43	96.00	92.00	86.89	97.25	92.00	54.92	90.54	68.00
TL	100	100.00	100.00	100.00	100.00	100.00	100.00	100.00	100.00	73.33	100.00	85.00
BA	75.00	100.00	86.00	73.68	100.00	85.00	75.44	100.00	86.00	56.14	94.12	70.00
TB	87.88	96.67	92.00	87.50	97.00	92.00	93.10	96.43	95.00	79.31	92.00	85.00
LL	80.00	100.00	89.00	83.33	100.00	91.00	91.67	100.00	96.00	50.00	100.00	67.00
CM	69.23	100.00	82.00	74.07	100.00	85.00	82.14	100.00	90.00	75.00	95.45	84.00
OA %		95.51			96.00			96.00			90.00	
Kappa %		91.00			93.00			93.00			80.00	

* Where AS*: Acacia seyal* Delile; CoH*: Combretum hartmannianum* Schweinf.; SS: *Sterculia setigera* Delile; DC: *Dichrostachys cinerea* (L.) Wight & Arn.; ASe*: Acacia senegal* (L.) Willd.; TL*: Terminalia laxiflora* Engl.; BA: *Balanites aegyptiaca* (L.) Delile; TB*: Terminalia brownii* Fresen.; LL*: Lonchocarpus laxiflorus* Guill. & Perr.; CM*: Combretum molle* R.Br. ex G.Don.

Table 4. Accuracy Assessment of Machine Learning Classifiers (RF, SVM, CART, Ensemble) for Dominant Tree Species Identification in 2013.

Species	RF			SVM			CART			Ensemble		
	PA (%)	UA (%)	F1-Score	PA (%)	UA (%)	F1-Score	PA (%)	UA (%)	F1-Score	PA (%)	UA (%)	F1-Score
AS	96.00	88.40	92.00	96.91	90.06	93.00	96.61	90.42	93.00	91.05	78.88	85.00
CoH	86.55	89.42	88.00	87.91	92.06	90.00	88.4	91.68	90.00	73.84	73.38	74.00
SS	89.57	89.73	90.00	91.22	91.54	91.00	91.46	91.46	91.00	82.74	78.95	81.00
DC	82.47	89.39	86.00	87.62	91.24	89.00	89.05	91.79	90.00	63.68	81.53	72.00
ASe	78.17	93.33	85.00	82.35	93.90	88.00	81.87	94.05	88.00	52.33	84.17	65.00
BA	80.88	98.21	89.00	87.01	98.53	92.00	85.9	98.53	92.00	55.13	89.58	68.00
AP	79.49	96.88	87.00	82.28	98.48	90.00	81.25	97.01	88.00	55.00	88.00	68.00
LF	86.30	96.92	91.00	85.71	96.43	91.00	89.06	96.61	93.00	57.81	92.5.00	71.00

CM	74.47	100.00	85.00	72.73	100.00	84.00	76.19	100.00	86.00	47.62	100.00	65.00
ZS	68.92	100.00	82.00	67.69	100.00	81.00	72.97	100.00	84.00	50.00	97.37	66.00
BL	77.61	96.30	86.00	80.88	96.49	88.00	82.19	96.77	89.00	41.10	78.95	54.00
OA %		90.00			92.00			92.00			79.00	
Kappa %		86.00			88.00			88.00			70.00	

* Where AS: *Acacia seyal* Delile; CoH*: Combretum hartmannianum* Schweinf.; SS: *Sterculia setigera* Delile; DC*: Dichrostachys cinerea* (L.) Wight & Arn.; ASe*: Acacia senegal* (L.) Willd.; BA*: Balanites aegyptiaca* (L.) Delile; AP*: Acacia polyacantha* Willd.; LF*: Lannea fruticosa* (Hochst. ex A.Rich.) Engl.; CM*: Combretum molle* R.Br. ex G.Don; ZS*: Ziziphus spina-christi* (L.) Desf.; BL*:* Bareland.

Table 5. Accuracy Assessment of Machine Learning Classifiers (RF, SVM, CART, Ensemble) for Dominant Tree Species Identification in 2018.

Species	RF			SVM			CART			Ensemble		
	PA (%)	UA (%)	F1-Score	PA (%)	UA (%)	F1-Score	PA (%)	UA (%)	F1-Score	PA (%)	UA (%)	F1-Score
AS	97.12	86.56	92.00	97.74	88.85	93.00	90.34	88.43	89.00	92.26	68.45	79.00
CoH	88.79	87.69	88.00	90.49	89.61	90.00	83.68	83.68	84.00	63.04	68.05	65.00
SS	78.71	91.39	85.00	84.39	93.38	89.00	77.23	83.27	80.00	52.48	79.1	63.00
DC	82.74	95.88	89.00	86.34	96.72	91.00	78.92	82.56	81.00	48.53	82.5	61.00
ASe	75.27	97.16	85.00	79.6	98.77	88.00	77.16	83.52	80.00	37.06	84.88	52.00
TB	76.74	100.00	87.00	77.27	100.00	87.00	74.36	72.50	73.00	43.59	85.00	58.00
AP	67.16	95.74	79.00	75.64	98.33	86.00	73.42	78.38	76.00	41.77	76.74	54.00
BA	75.82	100.00	86.00	80.00	100.00	89.00	73.63	76.14	75.00	30.77	87.50	46.00
LF	78.21	100.00	88.00	84.93	100.00	92.00	75.27	76.09	76.00	41.94	84.78	56.00
ZS	78.95	98.36	88.00	82.43	98.39	90.00	88.16	76.14	82.00	43.42	82.50	57.00
BL	73.42	100.00	85.00	75.34	100.00	86.00	84.51	77.92	81.00	39.44	90.32	55.00
OA %		89.00			91.00			85.00			71.00	
Kappa %		84.00			87.00			79.00			55.00	

* Where AS: *Acacia seyal* Delile; CoH: *Combretum hartmannianum* Schweinf.; SS: *Sterculia setigera* Delile; DC: *Dichrostachys cinerea* (L.) Wight & Arn.; ASe: *Acacia senegal* (L.) Willd.; TB: *Terminalia brownii* Fresen.; BA: *Balanites aegyptiaca* (L.) Delile; AP: *Acacia polyacantha* Willd.; LF: *Lannea fruticosa* (Hochst. ex A.Rich.) Engl.; ZS: *Ziziphus spina-christi* (L.) Desf.; BL: Bareland.

Table 6. Accuracy Assessment of Machine Learning Classifiers (RF, SVM, CART, Ensemble) for Dominant Tree Species Identification in 2021.

Species	RF			SVM			CART			Ensemble		
	PA (%)	UA (%)	F1-Score	PA (%)	UA (%)	F1-Score	PA (%)	UA (%)	F1-Score	PA (%)	UA (%)	F1-Score
AS	95.6	86.95	91.00	96.06	89.05	92.00	96.12	89.98	93.00	91.41	72.01	81.00
CoH	78.24	94.97	86.00	82.91	95.38	89.00	81.91	95.88	88.00	49.25	77.17	60.00
SS	94.44	78.49	86.00	95.61	81.43	88.00	95.63	83.47	89.00	87.95	57.84	70.00
ASe	77.78	94.79	85.00	80.87	95.88	88.00	87.20	97.32	92.00	60.00	88.24	71.00
BA	84.43	90.35	87.00	87.43	91.85	90.00	88.67	92.24	90.00	64.64	76.97	70.00
TB	77.87	96.94	86.00	83.04	96.88	89.00	80.49	97.06	88.00	37.40	90.2	53.00
LF	79.59	85.25	82.00	81.73	88.46	85.00	84.58	87.63	86.00	48.26	69.78	57.00
AN	81.9	89.32	85.00	84.38	91.22	88.00	84.95	90.64	88.00	52.35	74.55	62.00
AM	75.41	97.87	85.00	79.67	98.00	88.00	78.29	98.06	87.00	41.09	88.33	56.00
TL	76.77	93.83	84.00	79.00	94.05	86.00	81.25	95.12	88.00	53.12	80.95	64.00
BL	80.87	92.5	86.00	84.88	95.24	90.00	87.68	94.15	90.80	49.86	76.32	60.00
OA %		87.00			89.00			90.00			69.00	
Kappa %		85.00			87.00			88.00			63.00	

* Where AS: *Acacia seyal* Delile; CoH: *Combretum hartmannianum* Schweinf.; SS: *Sterculia setigera* Delile; ASe: *Acacia senegal* (L.) Willd.; TB: *Terminalia brownii* Fresen.; BA: *Balanites aegyptiaca* (L.) Delile; LF: *Lannea fruticosa* (Hochst. ex A.Rich.) Engl.; TL: *Terminalia laxiflora* Engl.; AM: *Acacia mellifera* (Vahl) Benth.; AN: *Acacia nubica* Benth.; BL: Bareland.

Across all study years, SVM and RF demonstrated the most consistent and reliable performance, achieving high OA, Kappa, and MCC values. CART showed comparable performance in several cases but exhibited greater variability, particularly for minority and spectrally ambiguous species. In contrast, the ensemble classifier consistently produced lower performance across all evaluation metrics, including MCC, indicating reduced robustness under class imbalance conditions.

While OA and Kappa indicated generally high classification accuracy, MCC provided a more balanced evaluation by incorporating all elements of the confusion matrix. The MCC results revealed a gradual decline in classification separability from 2008 to 2021, suggesting increasing spectral overlap, structural heterogeneity, and ecological complexity over time.

3.2.1. Accuracy Performance in 2008 (Landsat 5 TM)

The classification accuracy for 2008 is presented in Table 3. Overall, the three individual classifiers (RF, SVM, and CART) demonstrated consistently high performance, with overall accuracy exceeding 95.00% and Kappa coefficients above 90.00%. Among them, SVM and CART achieved slightly higher agreement levels, while RF provided comparably stable results. In contrast, the ensemble classifier showed lower performance (OA ≈ 90.00%, $\kappa \approx 80.00\%$), indicating that simple majority voting did not enhance classification accuracy relative to individual models.

Consistent with the MCC results (Table 2), all individual classifiers achieved very high balanced performance in 2008 (MCC > 0.91), indicating excellent class separability and minimal confusion among dominant species.

At the species level, dominant and structurally distinct species, particularly *A. seyal* and *T. laxiflora*, were classified with near-perfect accuracy across all individual classifiers. Secondary species, including *C. hartmannianum*, *S. setigera*, *A. senegal*, and *T. brownii*, also achieved high classification accuracy.

In contrast, species with lower canopy dominance and higher spectral overlap, such as *D. cinerea*, *B. aegyptiaca*, *L. laxiflorus*, and *C. molle*, exhibited greater variability in classification performance. The ensemble classifier consistently produced lower class-level accuracy, suggesting that unweighted majority voting amplified shared misclassification patterns.

3.2.2. Accuracy Performance in 2013 (Landsat 8 OLI)

The classification results for 2013 are summarized in Table 4. Overall, RF, SVM, and CART showed strong and comparable performance, with OA values between 90.00% and 92.00% and Kappa coefficients between 86.00% and 88.00%. The ensemble classifier produced lower performance (OA = 79.00%, $\kappa = 70.00\%$).

As indicated by the MCC results (Table 2), classification performance remained strong in 2013 (MCC ≈ 0.85–0.88), although a slight decline relative to 2008 suggests increased spectral complexity and class overlap.

At the class level, dominant species such as *A. seyal*, *S. setigera*, and *L. fruticosa* maintained high classification accuracy. Secondary species also showed stable performance, particularly under SVM and CART.

However, spectrally ambiguous classes, including *C. molle*, *Z. spina-christi*, and bareland, exhibited greater variability. The ensemble model again produced lower performance, confirming reduced effectiveness under mixed-class conditions.

3.2.3. Accuracy Performance in 2018 (Sentinel-2 MSI)

The accuracy assessment for 2018 is presented in Table 5. SVM achieved the highest performance (OA = 91.00%, κ = 87.00%), followed by RF (OA = 89.00%, κ = 84%). CART showed moderate performance, while the ensemble classifier produced the lowest results.

The MCC results (Table 2) show that SVM achieved the highest balanced performance (MCC = 0.8669), followed by RF, while CART exhibited a noticeable decline (MCC = 0.7411). This indicates increased sensitivity of CART to class imbalance and spectral overlap under higher-resolution Sentinel-2 data.

At the species level, dominant species (*A. seyal*, *C. hartmannianum*, and *S. setigera*) were classified more accurately by SVM and RF, reflecting improved spectral discrimination. However, minor species showed greater variability across classifiers.

The ensemble model again produced consistently lower performance, confirming that majority voting did not effectively resolve classification uncertainty.

3.2.4. Accuracy Performance in 2021 (Sentinel-2 MSI)

The classification results for 2021 are summarized in Table 6. CART achieved the highest performance (OA = 90.00%, κ = 88.00%), followed by SVM and RF. The ensemble classifier showed the lowest performance.

As reflected in the MCC results (Table 2), CART achieved the highest balanced performance in 2021 (MCC = 0.8584), followed by SVM and RF, while the ensemble classifier remained substantially weaker (MCC = 0.5197). This pattern suggests that CART was more effective in capturing complex class boundaries under increasing ecological heterogeneity.

At the class level, dominant species (*A. seyal*, *S. setigera*, and *B. aegyptiaca*) maintained high classification accuracy. Secondary species exhibited greater variability, particularly under the ensemble model.

Overall, the 2021 results confirm that individual classifiers remained robust, while the ensemble approach continued to underperform in resolving intermediate and rare species.

3.3. Comparison of Algorithm Performance for Dominant Tree Species Mapping

Across all study years, RF and SVM demonstrated the most stable and consistent performance for dominant tree species mapping, achieving high overall accuracy, strong Kappa agreement, and balanced class-level metrics (PA, UA, and F1-score). These models also showed greater robustness in handling class imbalance, maintaining relatively high performance for both dominant and less-represented species. This pattern was further supported by the Matthews Correlation Coefficient (MCC), which consistently indicated stronger predictive reliability for RF and SVM compared with other approaches, particularly under multi-class and imbalanced conditions.

CART produced competitive results in several years, particularly in 2008, 2013, and 2021, where its overall accuracy approached that of RF and SVM. However, its performance was less stable across classes, with increased variability observed for intermediate and rare species. This reflects the inherent limitations of single decision-tree models in capturing complex, non-linear relationships in heterogeneous dryland environments.

In contrast, the ensemble classifier consistently underperformed relative to the individual classifiers across all evaluation metrics, including OA, Kappa, F1-score, and MCC.

The ensemble model showed a marked reduction in class-level accuracy, particularly for minority species, indicating reduced sensitivity to less-represented classes.

This pattern suggests that the unweighted majority voting strategy did not introduce sufficient predictive diversity to improve classification outcomes. Instead, it frequently amplified shared misclassification tendencies among the base classifiers, particularly in areas characterized by spectral overlap and mixed canopy conditions. As a result, classification uncertainty was not reduced but rather propagated across the ensemble outputs.

Overall, the results demonstrate that individual classifiers, particularly RF and SVM, provided more reliable, stable, and ecologically meaningful classification outputs than the ensemble model under the present framework. These findings highlight the importance of model selection and ensemble design in dryland forest applications, where spectral complexity and class imbalance pose significant challenges to accurate species discrimination.

3.4. Variable Importance and Feature Contribution Across Classifiers

Variable importance analysis based on SHAP revealed consistent patterns across all study years, with spectral bands in the red, near-infrared (NIR), and shortwave infrared (SWIR) regions emerging as the most influential predictors, followed by NDVI-derived variables. These predictors collectively capture canopy structure, vegetation vigor, and moisture sensitivity, which are essential for species discrimination in dryland forest environments.

Topographic variables derived from DEM were included in the modeling framework; however, their contribution was negligible, and they did not appear among the top-ranked SHAP features, indicating a limited role in species discrimination compared to spectral and vegetation index variables.

In 2008 and 2013, Landsat-based classifications were mainly driven by NIR and SWIR bands, together with NDVI variables, indicating the importance of structural and moisture-related information for separating woody species. In 2018 and 2021, Sentinel-2 variables became more prominent, particularly NIR- and SWIR-related bands and several NDVI layers, reflecting the improved spectral detail of the sensor. Across all years, NDVI remained consistently important, especially for distinguishing dominant from secondary species.

A stable core group of predictors was consistently identified across all years. The most influential variables included NIR and SWIR bands (e.g., SR_B6/B8, SR_B7/B8_1, B11, B12) together with NDVI variants (e.g., NDVI1, NDVI2, NDVI6, NDVI10, and NDVI11). Their repeated dominance confirms that these variables are robust indicators of vegetation structure, vigor, and moisture conditions and are, therefore, highly suitable for long-term dryland forest monitoring.

Importantly, identical SHAP importance values were obtained across RF, SVM, and CART classifiers within each year, indicating that feature importance is primarily controlled by the intrinsic spectral characteristics of the input data rather than model-specific behavior. This consistency supports a unified interpretation of predictor contributions across classifiers.

Figure 3 presents the top-ranked SHAP features for each year. Because SHAP provides a model-agnostic measure of feature importance, the comparison is based on relative contribution magnitudes, ensuring a consistent and interpretable assessment of predictor relevance across time.

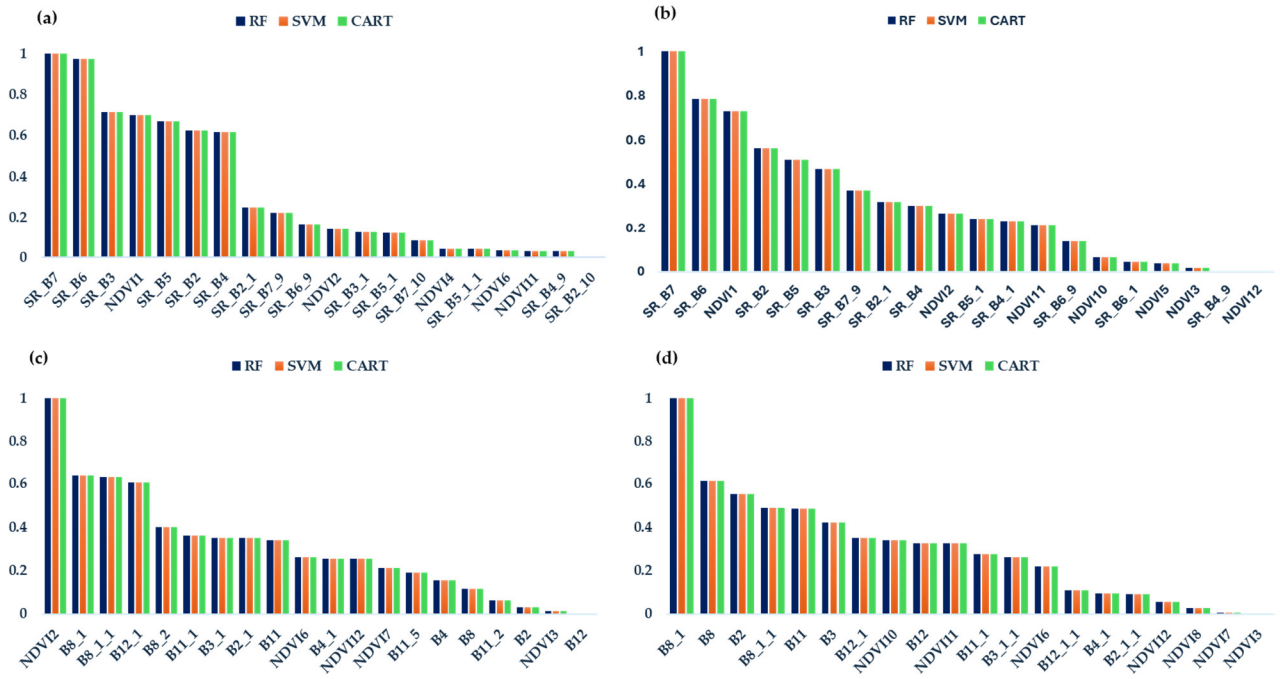

Figure 3. Top 20 feature importance across Random Forest (RF), Support Vector Machine (SVM), and Classification and Regression Tree (CART) classifiers derived using SHAP analysis for (**a**) 2008, (**b**) 2013, (**c**) 2018, and (**d**) 2021. Consistent patterns of variable importance are observed across all study years.

3.5. Spatial Distribution of Dominant Tree Species

The spatial distribution maps revealed coherent but algorithm-dependent patterns in the composition of dominant tree species across the study period. In all years, *A. seyal* occupied the largest proportion of the reserve, particularly in central and lowland areas, confirming its dominant structural role in the forest. In contrast, *S. setigera* and *C. hartmannianum* showed more fragmented and spatially variable distributions, often concentrated in transitional zones or areas likely influenced by disturbance and local environmental heterogeneity. Minor species were generally restricted to localized patches and were more consistently mapped by RF and SVM than by CART and the ensemble classifier, which tended to produce greater fragmentation and less spatially coherent patterns.

3.5.1. Spatial Distribution in 2008

The 2008 maps (Figure 4; Table 7) show strong agreement among classifiers in identifying *Acacia seyal* (Delile) as the dominant species, occupying approximately 70.00–74.00% of the reserve. This close agreement indicates that the species was both structurally dominant and spectrally well defined in the 2008 dataset. *S. setigera* represented the second most extensive species, although its estimated area varied among classifiers, suggesting higher sensitivity to class boundary definition and spectral overlap. *C. hartmannianum* occupied a smaller but clearly detectable proportion of the landscape.

Table 7. Estimated Area (ha) and Relative Proportion (%) of Dominant Tree Species in the Study Area Derived from RF, SVM, CART, and Ensemble Classifications in 2008.

Species	RF		SVM		CART		Ensemble	
	Area (ha)	%	Area (ha)	%	Area (ha)	%	Area (ha)	%
A. seyal	3372.81	71.29	3313.92	70.05	3313.92	70.05	3482.36	73.61
C. hartmannianum	250.24	5.29	193.35	4.09	193.35	4.09	222.92	4.71
S. setigera	979.79	20.71	1144.10	24.18	1144.10	24.18	887.99	18.77

D. cinerea	9.86	0.21	0.68	0.01	0.68	0.01	17.77	0.38
A. Senegal	77.64	1.64	64.57	1.36	64.57	1.36	69.87	1.48
T. laxiflora	3.09	0.07	0.98	0.02	0.98	0.02	3.41	0.07
B. aegyptiaca	13.71	0.29	4.14	0.09	4.14	0.09	18.56	0.39
T. brownii	13.55	0.29	6.93	0.15	6.93	0.15	13.31	0.28
L. laxiflorus	4.44	0.09	0.30	0.01	0.30	0.01	7.00	0.15
C. molle	5.95	0.13	2.11	0.04	2.11	0.04	7.88	0.17

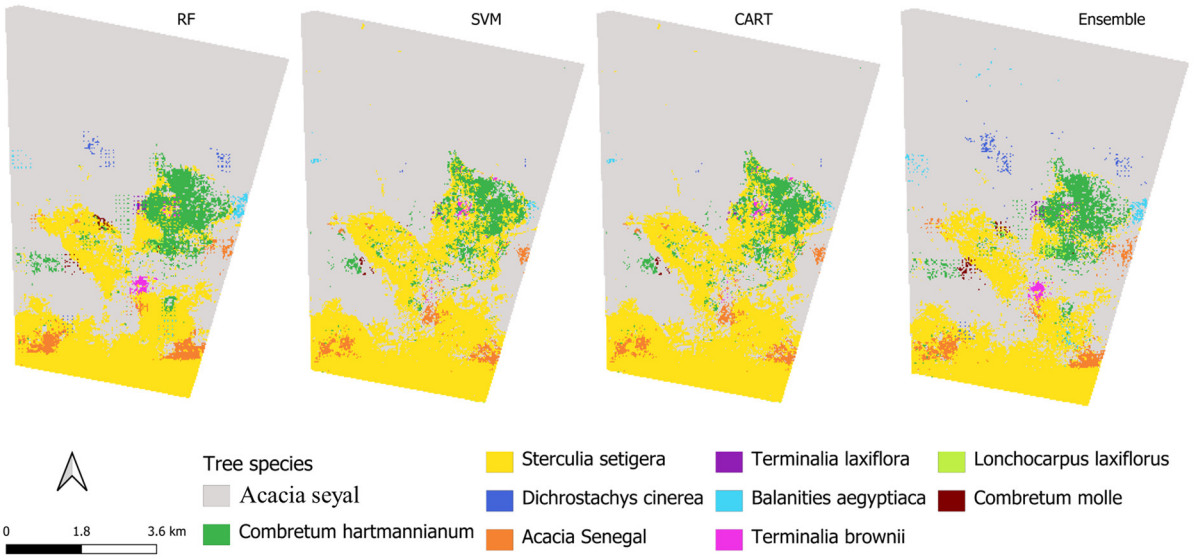

Figure 4. Spatial distribution of dominant tree species in ENFR using RF, SVM, CART, and Ensemble models in 2008.

Minor species consistently accounted for very small proportions of the total area. However, the ensemble model tended to assign slightly larger areas to some rare classes than RF, SVM, and CART, indicating a tendency toward overgeneralization during majority voting. Overall, the 2008 results suggest relatively stable identification of dominant species, with uncertainty concentrated mainly in minor and spectrally similar classes.

3.5.2. Spatial Distribution in 2013

In 2013 (Figure 5; Table 8), *A. seyal* remained the dominant species across all classifiers, although its proportional coverage decreased relative to 2008. *S. setigera* continued to represent the second most extensive class, while *C. hartmannianum* increased in relative importance compared with the previous period. This pattern suggests a shift in canopy composition rather than abrupt structural loss.

Table 8. Estimated Area (ha) and Relative Proportion (%) of Dominant Tree Species in the Study Area Derived from RF, SVM, CART, and Ensemble Classifications in 2013.

Species Name	RF		SVM		CART		Ensemble	
	Area (ha)	%	Area (ha)	%	Area (ha)	%	Area (ha)	%
A. seyal	2856.01	60.37	3187.33	67.37	3187.33	67.37	3021.29	63.86
C. hartmannianum	616.59	13.03	409.01	8.65	409.01	8.65	605.10	12.79
S. setigera	841.63	17.79	976.23	20.63	976.23	20.63	709.99	15.01
D. cinerea	161.00	3.40	77.75	1.64	77.75	1.64	134.40	2.84
A. Senegal	89.96	1.90	31.11	0.66	31.11	0.66	83.62	1.77
B. aegyptiaca	32.47	0.69	3.69	0.08	3.69	0.08	39.84	0.84
A. polycantha	29.53	0.62	11.90	0.25	11.90	0.25	27.84	0.59

L. fruticosa	55.68	1.18	6.93	0.15	6.93	0.15	47.81	1.01
C. molle	8.51	0.18	4.07	0.09	3.77	0.08	11.03	0.23
Z. spina-christi	14.77	0.31	20.19	0.43	20.19	0.43	23.20	0.49
Bareland	24.94	0.53	2.86	0.06	3.16	0.07	26.97	0.57

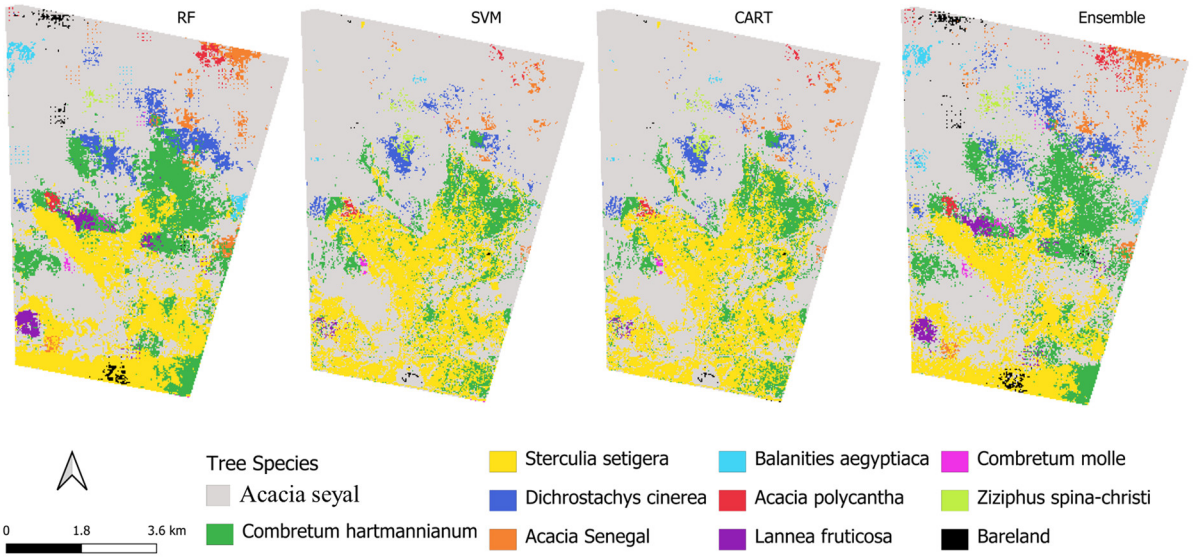

Figure 5. Spatial distribution of dominant tree species in ENFR using RF, SVM, CART, and Ensemble models in 2013.

As in 2008, algorithm-dependent differences were more evident for secondary and minor species than for the dominant class. RF tended to assign relatively larger areas to *C. hartmannianum*, whereas SVM and CART gave comparatively larger estimates for *Sterculia setigera*. The ensemble model again produced slightly higher area estimates for several rare classes and bareland, indicating reduced stability in the treatment of sparse or mixed classes. Despite these differences, the broad spatial structure of the reserve remained consistent across models.

3.5.3. Spatial Distribution in 2018

The 2018 maps (Figure 6; Table 9) displayed greater divergence among classifiers than in earlier years. RF and SVM produced nearly identical estimates for the main species, with *A. seyal* remaining dominant and *C. hartmannianum* becoming much more prominent than in previous years. In contrast, CART assigned a substantially lower proportion to *A. seyal* and relatively higher areas to several minor species, reflecting greater sensitivity to class imbalance and spectral overlap. The ensemble model produced the largest estimate for *A. seyal* but lower estimates for *C. hartmannianum* and *S. setigera*, suggesting that hard voting did not reconcile model differences effectively.

Table 9. Estimated Area (ha) and Relative Proportion (%) of Dominant Tree Species in the Study Area Derived from RF, SVM, CART, and Ensemble Classifications in 2018.

Species	RF		SVM		CART		Ensemble	
	Area (ha)	%	Area (ha)	%	Area (ha)	%	Area (ha)	%
A. seyal	3230.70	68.29	3230.70	68.29	2235.87	47.26	3500.48	73.99
C. hartmannianum	1029.13	21.75	1029.13	21.75	928.53	19.63	750.44	15.86
S. setigera	219.01	4.63	219.01	4.63	402.56	8.51	157.51	3.33
D. cinerea	103.14	2.18	103.14	2.18	275.83	5.83	105.94	2.24
A. Senegal	75.41	1.59	75.41	1.59	237.41	5.02	68.56	1.45

T. brownii	5.35	0.11	5.35	0.11	66.45	1.40	19.70	0.42
A. polycantha	8.81	0.19	8.81	0.19	107.97	2.28	28.37	0.60
B. aegyptiaca	14.69	0.31	14.69	0.31	141.42	2.99	22.94	0.48
L. fruticosa	28.10	0.59	28.10	0.59	109.55	2.32	31.61	0.67
Z. spina-christi	8.66	0.18	8.66	0.18	127.63	2.70	28.19	0.60
Bareland	8.06	0.17	8.06	0.17	97.87	2.07	17.34	0.37

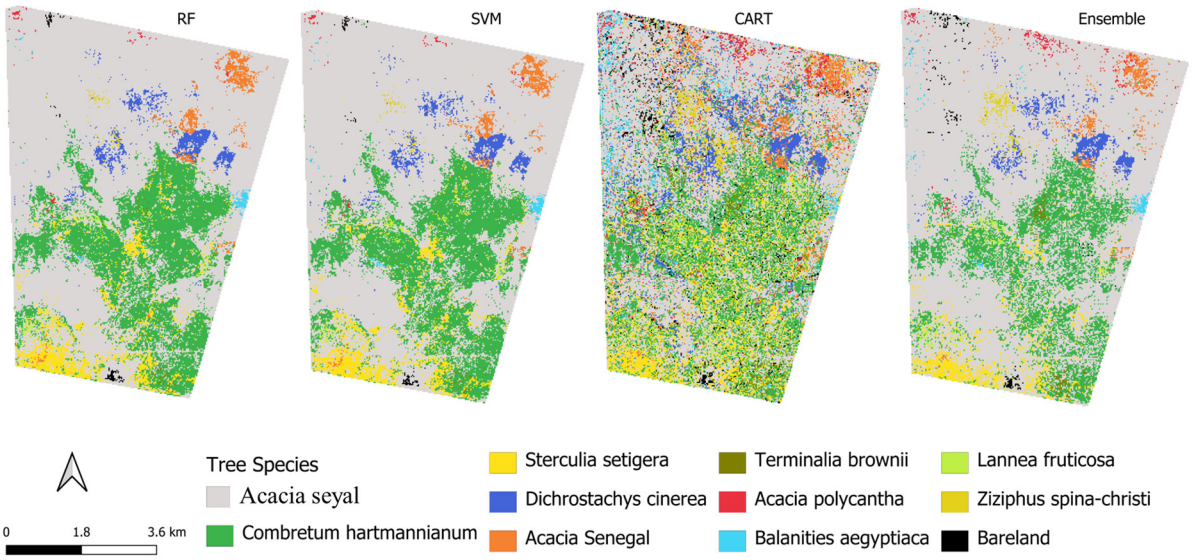

Figure 6. Spatial distribution of dominant tree species in ENFR using RF, SVM, CART, and Ensemble models in 2018.

Minor species remained limited in spatial extent but showed stronger inter-model variability than in 2008 and 2013. CART in particular tended to assign larger areas to sparse classes, reinforcing the pattern observed in the accuracy assessment that single-tree models were more sensitive to minor-class overestimation. Overall, the 2018 results suggest that the introduction of Sentinel-2 data improved discrimination for dominant species but did not eliminate uncertainty for secondary and low-abundance taxa.

3.5.4. Spatial Distribution in 2021

In 2021 (Figure 7; Table 10), the maps indicate a marked restructuring of species dominance. *A. seyal* remained a major species, but its proportional coverage declined substantially compared with earlier years. In contrast, *S. setigera* showed a strong increase and emerged as a co-dominant or dominant class, depending on the classifier. This shift was consistent enough across models to suggest a real compositional change rather than a purely methodological artifact.

Table 10. Estimated Area (ha) and Relative Proportion (%) of Dominant Tree Species in the Study Area Derived from RF, SVM, CART, and Ensemble Classifications in 2021.

Species	**RF**		**SVM**		**CART**		**Ensemble**	
	Area (ha)	**%**	**Area (ha)**	**%**	**Area (ha)**	**%**	**Area (ha)**	**%**
A. seyal	1619.61	34.23	1598.85	33.79	1598.85	33.79	1784.91	37.73
C. hartmannianum	104.63	2.21	390.07	8.24	390.07	8.24	324.83	6.87
S. setigera	1821.20	38.49	1315.93	27.81	1315.93	27.81	1731.68	36.60
A. Senegal	62.52	1.32	186.93	3.95	186.93	3.95	74.25	1.57
B. aegyptiaca	336.73	7.12	328.89	6.95	328.89	6.95	292.09	6.17
T. brownii	24.11	0.51	153.48	3.24	153.48	3.24	42.20	0.89

L. fruticosa	190.51	4.03	164.26	3.47	164.26	3.47	132.03	2.79
A. nubica	274.66	5.81	212.93	4.50	212.93	4.50	163.73	3.46
A. mellifera	31.64	0.67	125.00	2.64	125.00	2.64	24.17	0.51
T. laxiflora	47.01	0.99	107.37	2.27	107.37	2.27	31.17	0.66
Bareland	218.46	4.62	147.38	3.12	147.38	3.12	130.02	2.75

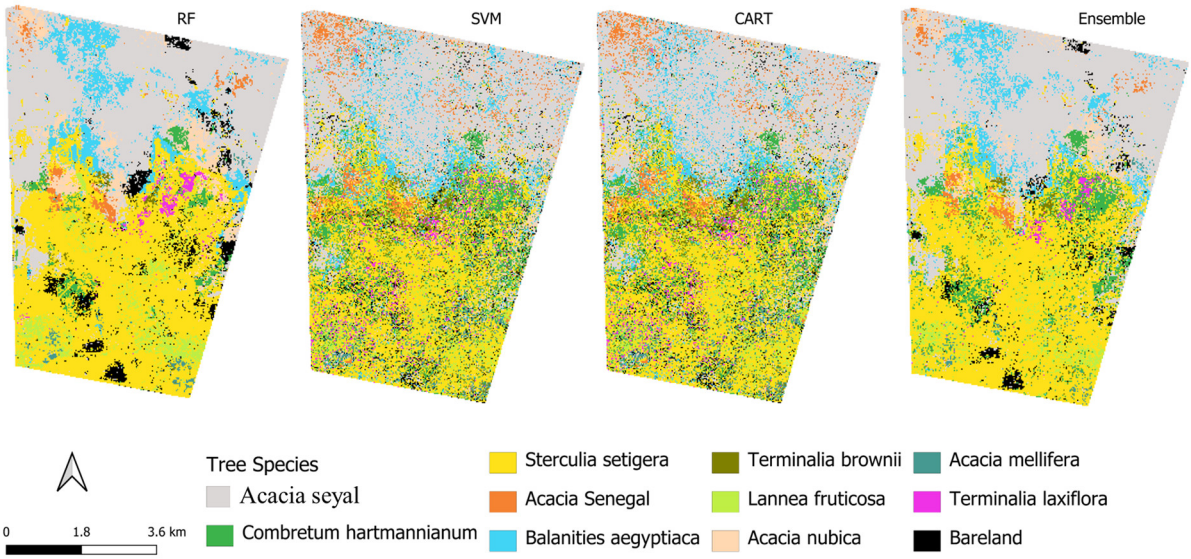

Figure 7. Spatial distribution of dominant tree species in ENFR using RF, SVM, CART, and Ensemble models in 2021.

C. hartmannianum, which had increased in 2018, showed reduced coverage in 2021. Minor species remained limited in extent, although CART continued to assign relatively larger areas to some sparse classes, especially compared with RF and SVM. Bareland remained low across all classifiers, indicating that the observed changes were more strongly associated with shifts in species composition than with widespread conversion to non-vegetated land.

3.6. Temporal Dynamics of Dominant Tree Species (2008–2021)

The multi-temporal analysis revealed pronounced changes in species composition and dominance structure between 2008 and 2021 (Table 11). Across all classifiers, *A. seyal* remained the dominant species from 2008 through 2018, but its proportional cover declined sharply by 2021. Although the magnitude of decline varied among classifiers, all models captured the same overall pattern, indicating a substantial reduction in the relative dominance of this species over time.

Table 11. Relative area (%) of the three dominant species in 2008, 2013, 2018, and 2021 derived from RF, SVM, CART, and ensemble classifications.

Year	Species	RF (%)	SVM (%)	CART (%)	Ensemble (%)
2008	*A. seyal*	71.29	70.05	70.05	73.61
	S. setigera	20.71	24.18	24.18	18.77
	C. hartmannianum	5.29	4.09	4.09	4.71
2013	*A. seyal*	60.37	67.37	67.37	63.86
	S. setigera	17.79	20.63	20.63	15.01
	C. hartmannianum	13.03	8.65	8.65	12.79
2018	*A. seyal*	68.29	68.29	47.26	73.99
	S. setigera	4.63	4.63	8.51	3.33

	C. hartmannianum	21.75	21.75	19.63	15.86
	A. seyal	34.23	33.79	33.79	37.73
2021	*S. setigera*	38.49	27.81	27.81	36.6
	C. hartmannianum	2.21	8.24	8.24	6.87

In contrast, *S. setigera* showed a more dynamic trajectory. It was consistently the second most important species in 2008 and 2013, declined in 2018, and then increased sharply in 2021. This late increase suggests a major shift in species composition and indicates that *S. setigera* became increasingly important in the later phase of the study period. *C. hartmannianum* followed a different trajectory, increasing from 2008 to 2018 before declining in 2021. Taken together, these patterns indicate substantial temporal reorganization in the composition of the dominant canopy.

Minor species remained relatively limited in areal extent throughout the study period, although CART occasionally assigned higher proportions to rare classes than RF and SVM, indicating greater sensitivity to class imbalance. Bareland remained consistently low in all years, suggesting that the principal ecological change was not widespread canopy loss or land conversion but rather species replacement and compositional restructuring within the forest.

3.7. Error-Adjusted Area Estimation of Top Three Species and Uncertainty Analysis

Error-adjusted area estimates revealed consistent differences from map-based values across all years and classifiers, providing a more robust representation of species dominance and associated uncertainty (Table 12). In general, adjustment reduced the dominance of *Acacia seyal* while increasing the relative contribution of secondary species, particularly *Sterculia setigera*.

Table 12. Map-based and error-adjusted area estimates (%) with confidence limits (±CL) for dominant tree species across RF, SVM, CART, and ensemble classifiers (2008–2021).

Year	Species	RF		SVM		CART		Ensemble	
		Area Adj (%)	±CL	Area Adj (%)	±CL	Area Adj (%)	±CL	Area Adj (%)	±CL
2008	*A. seyal*	68.70	±2.10	68.00	±2.30	68.20	±2.20	61.30	±3.50
	S. setigera	19.30	±1.80	22.70	±2.10	22.50	±2.00	16.30	±2.40
	C. hartmannianum	4.90	±0.90	3.80	±0.80	3.90	±0.80	4.10	±1.20
2013	*A. seyal*	53.40	±3.20	60.70	±2.80	60.50	±2.90	50.30	±3.90
	S. setigera	16.00	±2.10	18.80	±2.20	18.60	±2.10	11.80	±2.60
	C. hartmannianum	11.60	±2.00	8.00	±1.70	8.10	±1.80	9.40	±2.50
2018	*A. seyal*	59.10	±3.00	60.70	±2.80	41.70	±3.50	50.60	±4.20
	S. setigera	4.20	±1.00	4.40	±1.10	7.80	±1.50	2.90	±1.30
	C. hartmannianum	19.10	±2.40	19.50	±2.30	16.40	±2.60	10.80	±3.00
2021	*A. seyal*	29.80	±2.70	30.00	±2.60	30.20	±2.60	27.20	±3.20
	S. setigera	33.00	±3.10	25.40	±2.80	25.80	±2.90	29.30	±3.40
	C. hartmannianum	1.90	±0.80	7.50	±1.70	7.60	±1.80	5.00	±2.00

In 2008, *A. seyal* remained the dominant species, with adjusted values of approximately 68–69% under RF, SVM, and CART but lower under the ensemble model (61.3% ± 3.5). *S. setigera* increased slightly after adjustment (up to 22.7% ± 2.1), indicating underestimation in map-based results, while *C. hartmannianum* remained minor (3.8–4.9%) with low uncertainty.

By 2013, *A. seyal* declined to 50.3–60.7%, while *C. hartmannianum* increased, reaching 11.6% ± 2.0 under RF. Confidence limits widened (±2.8–3.9), reflecting increased

uncertainty. In 2018, divergence among classifiers was more pronounced, with RF and SVM showing consistent *A. seyal* dominance (~59–61%), whereas CART and ensemble produced lower estimates (41.7–50.6%). During this period, *C. hartmannianum* peaked (~19–20%), while *S. setigera* declined (2.9–7.8%).

In 2021, a major shift in dominance structure was observed. *A. seyal* declined sharply to 27–30%, while *S. setigera* increased substantially, becoming dominant under RF (33.0% ± 3.1) and ensemble models (29.3% ± 3.4). *C. hartmannianum* declined again (1.9–7.6%) with wider uncertainty.

Overall, error-adjusted estimates confirm a significant transition from *A. seyal* dominance toward the increasing importance of *S. setigera*, with consistent patterns across classifiers and confidence limits.

4. Discussion

4.1. Performance of Machine Learning Algorithms for Dryland Tree Species Mapping

The comparative analysis showed that RF and SVM provided the most consistent and reliable performance for dominant tree species mapping in ENFR across all study years. Both classifiers achieved high overall accuracy, strong class-level performance, and consistently higher Matthews Correlation Coefficient (MCC) values, indicating robust predictive capability under multi-class and imbalanced conditions. This finding is consistent with previous remote sensing studies that identify RF and SVM as among the most robust methods for vegetation and tree species classification in heterogeneous landscapes [20,26,35,36,49,73,74]. Although CART also performed competitively in several years, its results were less stable than those of RF and SVM, especially for minor and spectrally overlapping classes. Similar patterns have been reported in studies showing that single-tree models are more sensitive to noise, class imbalance, and local decision errors than ensemble-based or margin-based classifiers [20,35,47,75–80].

The strong performance of RF can be attributed to its ability to handle high-dimensional predictors, non-linear relationships, and noisy training data while reducing overfitting through ensemble learning [35,79,80]. Likewise, SVM is well-suited for separating spectrally similar classes in complex feature space, which is particularly relevant in dryland ecosystems where sparse canopy cover and heterogeneous vegetation structure reduce class separability [20,36,70,78]. In contrast, the comparatively weaker performance of CART and the ensemble model indicates that simpler or less diverse models may be less effective in environments characterized by class imbalance and high spectral similarity [20,36,74]. The persistent underperformance of the ensemble approach further suggests that unweighted majority voting failed to introduce sufficient predictive diversity, instead amplifying shared misclassification patterns among base classifiers.

Importantly, the results also indicate a gradual decline in MCC from 2008 to 2021, reflecting reduced class separability and increasing spectral overlap, likely associated with structural degradation and growing ecological heterogeneity. Therefore, high overall accuracy alone does not fully represent ecological reliability, and classifier performance should be evaluated using balanced metrics and class-level consistency.

4.2. Influence of Sensor Type and Multi-Temporal Data on Classification Accuracy

Sensor type influenced classification performance, but it did not override the importance of algorithm selection. The transition from Landsat TM and OLI imagery (2008–2013) to Sentinel-2 MSI data (2018–2021) generally improved species discrimination, particularly for RF and SVM. This likely reflects the finer spatial resolution and enhanced spectral sensitivity of Sentinel-2, especially in the red-edge, NIR, and SWIR regions, which are known to capture variation in canopy structure, pigment content, and moisture status

[26,49,81,82]. These characteristics are especially valuable in dryland forests, where species often exhibit subtle spectral differences.

However, the results also demonstrate that improved sensor characteristics alone were not sufficient to ensure consistent classification outcomes. Despite the higher resolution of Sentinel-2, variability among classifiers persisted across OA, Kappa, F1-score, and MCC values, indicating that model structure and sensitivity to class imbalance remained critical determinants of performance. This finding is consistent with previous studies showing that algorithm design and decision boundary flexibility can have as much influence as sensor characteristics in spectrally complex environments [20,35,36]. Moreover, the observed decline in MCC from 2008 to 2021 suggests that increasing ecological heterogeneity and spectral overlap may partially offset the advantages of higher-resolution data.

In addition, differences in error-adjusted area estimates across sensors and classifiers highlight the role of classification uncertainty, particularly for secondary and minority species. This suggests that improved spectral detail may reveal greater ecological complexity rather than reduce classification ambiguity.

The multi-temporal design of the study provided further value by distinguishing persistent ecological patterns from year-specific classification effects. Given that dryland vegetation is strongly influenced by seasonal and interannual climatic variability, single-date assessments may lead to biased interpretations of species distribution [20,26,49]. Therefore, the multi-year framework enhances the robustness of long-term ecological inference.

4.3. Species-Area Estimates and Model Behavior

Clear and systematic differences were observed in how the classifiers estimated species area across all study years. RF generally produced conservative and stable area estimates, particularly for secondary and minor species, which is consistent with its documented robustness to multicollinearity, noisy predictors, and imbalanced training data [20,36]. SVM also produced ecologically plausible area estimates and reliably captured temporal trends, further supporting its suitability for complex vegetation discrimination [26,49]. In contrast, CART showed a greater tendency to overestimate some minor and fragmented classes, especially in the Sentinel-2 years, likely due to the sensitivity of single-tree models to local decision rules and imbalanced class distributions [20,35]. The ensemble model exhibited inconsistent behavior, often underestimating dominant classes while amplifying uncertainty in minority classes, reflecting the limitations of unweighted majority voting under shared classification errors.

Importantly, differences between map-based and error-adjusted area estimates highlight the influence of classification bias and uncertainty on ecological interpretation. The adjustment process consistently reduced the dominance of major species while increasing the relative contribution of secondary species, indicating that some classifiers tended to overpredict dominant classes. This pattern became more pronounced over time, coinciding with increasing uncertainty and wider confidence intervals, which reflect growing ecological heterogeneity and fragmentation.

These findings are critical because they demonstrate that high classification accuracy does not necessarily translate into reliable species-area estimation. The observed discrepancies between accuracy metrics and area estimates, together with the decline in MCC, suggest that classification uncertainty increased as class separability decreased. Therefore, in long-term ecological monitoring, reliance on summary accuracy metrics alone may lead to biased interpretations of species dominance and forest dynamics, and classifier evaluation should incorporate both spatial realism and uncertainty assessment.

4.4. Effectiveness of Ensemble Classification in Dryland Forest Mapping

Although ensemble classification is often proposed to improve robustness and reduce model-specific uncertainty, the unweighted hard-voting ensemble in this study consistently underperformed relative to RF and SVM. The ensemble frequently inflated the mapped area of dominant classes while producing less consistent and less reliable results for rare and spectrally ambiguous species. This indicates that majority voting did not effectively reduce classification uncertainty but instead amplified shared misclassification patterns among the component classifiers, particularly under conditions of class imbalance and spectral overlap.

This result is methodologically significant. RF already functions as an ensemble of decision trees, while CART provides limited additional predictive diversity due to its similar tree-based structure. As a result, combining RF, CART, and SVM did not introduce sufficient model heterogeneity to improve classification reliability through simple majority voting. This limitation is further reflected in the lower MCC values of the ensemble model, indicating reduced balanced predictive performance. Similar constraints of unweighted ensemble approaches have been reported in vegetation mapping studies, where correlated model errors reduce the expected benefits of ensemble aggregation [20,35]. Previous studies suggest that effective ensemble strategies require weighting schemes based on classifier confidence, probability outputs, or class-specific performance rather than equal voting [26,36].

4.5. Variable Importance and Predictor Relevance

The SHAP-based feature importance analysis showed that NIR, SWIR, and NDVI-related variables were consistently the most influential predictors across all study years, while DEM-derived variables contributed only marginally. This pattern is ecologically meaningful because NIR and SWIR bands are closely linked to canopy structure, moisture content, and vegetation biomass, whereas NDVI captures vegetation vigor and phenological variability [20,35]. These characteristics are particularly important for differentiating woody species in dryland ecosystems, where sparse canopy cover and heterogeneous vegetation structure often reduce spectral contrast among classes [26,49].

The persistent dominance of these variables across both Landsat and Sentinel-2 datasets confirms their robustness for long-term dryland forest monitoring. In particular, the strong contribution of NIR- and SWIR-related bands, together with multiple NDVI layers, indicates that species discrimination in ENFR is primarily controlled by functional and structural vegetation traits rather than terrain conditions alone. Although topographic variables were included in the modeling framework, their contribution remained weak, suggesting that terrain exerts only a limited influence on species separability within the study area, except in localized areas where it may affect soil moisture and microclimatic conditions [20,36].

Importantly, the identical SHAP importance patterns observed across RF, SVM, and CART indicate that predictor relevance was driven mainly by the intrinsic spectral properties of the input variables rather than classifier-specific behavior. This consistency strengthens the ecological interpretation of the selected predictors and supports their suitability for multi-temporal species mapping.

4.6. Ecological Interpretation of Dominant Tree Species Distribution

The long-term dominance of *A. seyal* across the study period confirms its central structural role within the dryland forest system. Its large proportional cover in 2008 and 2013, consistently detected across classifiers and supported by high classification accuracy and balanced MCC values, indicates a relatively stable and well-structured canopy under prevailing semi-arid conditions. Similar persistence of dominant woody species has been

reported in remote sensing studies where structurally extensive species exhibit strong spectral separability and classification consistency [20,26]. However, the marked decline in *A. seyal* by 2021, consistently observed across RF, SVM, and CART and confirmed by error-adjusted area estimates, indicates that this pattern is unlikely to be a classification artifact and instead reflects a substantial shift in forest composition [35,36].

In contrast, the pronounced increase in *S. setigera* by 2021 suggests a reorganization of canopy composition and dominance structure. The increase in secondary or disturbance-tolerant species is commonly associated with canopy opening, reduced competition, and increasing environmental stress in dryland ecosystems [20,35]. The temporal dynamics of *C. hartmannianum*, which increased up to 2018 and declined thereafter, further indicate species-specific responses to changing ecological conditions, likely reflecting differences in regeneration capacity and disturbance sensitivity [36,49].

Moreover, the increasing uncertainty in area estimates and the observed decline in MCC over time indicate growing spectral overlap and structural heterogeneity, consistent with progressive ecosystem degradation. Collectively, these results suggest a transition from *A. seyal*-dominated woodland toward a more heterogeneous and structurally simplified system, reflecting reduced ecological stability and resilience.

4.7. Spatiotemporal Changes Under Environmental and Anthropogenic Pressures

The observed spatiotemporal changes are consistent with the combined influence of climatic variability and anthropogenic pressure, although direct attribution remains limited. Dryland vegetation is highly sensitive to fluctuations in rainfall, temperature, and moisture availability, and its responses are often delayed and non-linear [20,26]. The progressive decline in classification separability, reflected by decreasing MCC values, together with increasing uncertainty in area estimates, suggests cumulative ecological stress rather than short-term variability, indicating a system undergoing gradual structural transformation.

At the same time, field evidence indicates that anthropogenic activities play a dominant role in shaping these dynamics. Illegal tree cutting and charcoal production contribute to the selective removal of mature trees, directly reducing the dominance of key species such as *A. seyal*. Overgrazing further constrains regeneration by limiting seedling establishment, promoting the increase in disturbance-tolerant species such as *S. setigera*. In addition, weak governance, limited enforcement, and strong socioeconomic dependence on forest resources contribute to sustained extraction pressure and localized degradation [8,16,18,66,67].

The observed reduction in dominant species, combined with the increase in secondary species, reflects a gradual degradation pathway characterized by compositional change rather than abrupt canopy loss [20,35,36]. The consistently low proportion of bareland supports this interpretation, indicating that structural simplification and fragmentation, rather than widespread land conversion, are the primary processes driving landscape change [20,26,49].

Environmental factors, including rainfall variability and prolonged dry periods, likely act as secondary stressors that amplify degradation processes by reducing regeneration success and increasing ecosystem vulnerability.

4.8. Implications for Forest Monitoring and Management

From an operational perspective, the results demonstrate that RF and SVM are effective tools for long-term dryland forest monitoring. Their consistent performance across sensors and years, combined with comparatively realistic species-area estimates and higher MCC values, highlights their robustness under class imbalance and increasing ecological complexity [20,26,35,36]. The observed decline in MCC over time further

emphasizes the importance of using balanced accuracy metrics, as reliance on overall accuracy alone may mask increasing classification uncertainty. The cloud-based implementation in GEE enhances the applicability of the framework by enabling reproducible, scalable, and cost-effective analysis in data-scarce regions [28,39–41]. However, the underperformance of the ensemble model indicates that simple aggregation strategies may not improve reliability and that careful model selection remains critical.

From a management perspective, the decline in *A. seyal* indicates the need for targeted conservation and restoration measures, including protection of mature seed trees, regulation of selective harvesting, and support for natural regeneration [35,36]. The concurrent increase in *S. setigera*, together with rising uncertainty and species redistribution, suggests a shift toward disturbance-driven dynamics rather than ecological recovery. Therefore, management strategies should prioritize maintaining species composition, structural diversity, and regeneration capacity, rather than focusing solely on total woody cover. Integrating remote sensing with field-based monitoring and error-adjusted area estimation would improve the detection of early degradation signals and support adaptive, evidence-based forest management [20,26,49].

4.9. Methodological Limitations and Uncertainty

Several remote sensing-related limitations should be acknowledged. First, the use of medium-resolution imagery (10–30 m) limits the ability to resolve fine-scale canopy heterogeneity and increases mixed-pixel effects, particularly in areas with fragmented vegetation and for spectrally similar species. This limitation is consistent with the observed variability in class-level performance and reduced separability among minor classes [35,49].

Second, spectral similarity among woody species with comparable canopy structure and phenological behavior remains a key challenge. The observed decline in MCC from 2008 to 2021 suggests increasing spectral overlap associated with structural degradation and ecological heterogeneity, which reduces the effectiveness of spectral-based discrimination even when higher-resolution Sentinel-2 data are used.

Third, the multi-sensor nature of the dataset introduces potential inconsistencies due to differences in spectral configuration and radiometric properties between Landsat and Sentinel-2. Although preprocessing and feature selection reduced these effects, residual differences may still influence the temporal comparability of classification results.

Fourth, class imbalance inherent in dryland ecosystems affects model performance, particularly for rare species. While RF and SVM demonstrated robustness, lower accuracy and higher uncertainty for minority classes remain unavoidable under current spectral constraints.

Finally, although SHAP analysis provided consistent identification of key predictors, the feature space remains limited to spectral and index-based variables. Incorporating additional data sources such as structural (LiDAR), microwave (SAR), or hyperspectral information would likely improve species discrimination, reduce uncertainty, and enhance the detection of subtle ecological changes in dryland forest systems [36,49,83].

5. Conclusions

This study developed and evaluated a multi-temporal and multi-sensor machine learning framework implemented in Google Earth Engine for mapping dominant tree species in Sudanese dryland forests. The results demonstrate that classification performance is primarily controlled by algorithm selection. Random Forest (RF) and Support Vector Machine (SVM) consistently provided the most stable, accurate, and transferable results across sensors and years, whereas Classification and Regression Trees (CART) showed greater sensitivity to class imbalance and spectral overlap. The unweighted ensemble

approach did not improve classification performance and often amplified errors in minority classes, indicating that simple majority voting is not suitable for structurally heterogeneous dryland ecosystems.

Sensor characteristics influenced classification outcomes, with Sentinel-2 improving species discrimination due to enhanced spatial and spectral resolution, particularly in the red-edge, NIR, and SWIR regions. However, these improvements did not eliminate inter-algorithm variability, confirming that model structure remains the dominant factor controlling classification reliability. The consistent importance of NDVI, NIR, and SWIR variables highlights their robustness for dryland vegetation monitoring.

Multi-temporal analysis revealed a progressive decline in classification separability, reflected by decreasing MCC values, indicating increasing spectral overlap and ecological complexity over time. A clear shift in species composition was observed, with a significant decline in *A. seyal* and increased dominance of *S. setigera*, supported by error-adjusted area estimates and uncertainty analysis. These patterns indicate a transition toward a more heterogeneous and structurally simplified ecosystem.

These changes are primarily driven by anthropogenic pressures, particularly illegal logging and overgrazing, with climatic variability acting as an amplifying factor. Overall, the study provides a robust, scalable, and reproducible framework for long-term dryland forest monitoring, supporting improved detection and interpretation of ecosystem change.

Author Contributions: Conceptualization, E.H.E.Y.; methodology, E.H.E.Y.; validation, E.H.E.Y.; formal analysis, E.H.E.Y.; investigation, E.H.E.Y.; data curation, E.H.E.Y.; writing—original draft preparation, E.H.E.Y.; writing—review and editing, E.H.E.Y., M.K. and K.C.; visualization, E.H.E.Y., M.K. and K.C.; supervision, K.C. All authors have read and agreed to the published version of the manuscript.

Funding: This research received funds from the project TKP2021-NVA-13, which was implemented with the support provided by the Ministry of Culture and Innovation of Hungary from the National Research, Development and Innovation Fund, financed under the TKP2021-NVA funding scheme.

Data Availability Statement: The data that support the findings of this study are available from the corresponding author upon reasonable request.

Acknowledgments: The authors gratefully acknowledge the colleagues and staff of the Institute of Geomatics and Civil Engineering at the University of Sopron for academic collaboration and support and their colleagues for their valuable support. Special thanks are extended to the Stipendium Hungaricum for providing a scholarship to the first author, the project TKP2021-NVA-13 for providing financial support for the publication of this paper, and the Department of Forest Resources Planning and Informatics, Technical University in Zvolen for their support and academic collaboration.

Conflicts of Interest: The authors declare no conflicts of interest.

Abbreviations

The following abbreviations are used in this manuscript:

LULC	Land Use/Land Cover
ENFR	Elnour Natural Forest Reserve
FAO	Food and Agriculture Organization
CART	Classification and Regression Trees
RF	Random Forest
SVM	Support Vector Machine
DEM	Digital Elevation Model
NDVI	Normalized Difference Vegetation Index

GEE	Google Earth Engine
TM	Thematic Mapper
OLI	Operational Land Imager
MSI	Multi-Spectral Instrument
RBF	Radial Basis Function
OA	Overall Accuracy
PA	Producer's Accuracy
UA	User's Accuracy

References

1. Agustino, S.; Mataya, B.; Senelwa, K.; Achigan-Dako, E.G. *Non-Wood Forest Products and Services for Socio-Economic Development: A Compendium for Technical and Professional Forestry Education*; The African Forest Forum: Nairobi, Kenya, 2011; 239p.
2. Osewe, E.O.; Popa, B.; Vacik, H.; Osewe, I.; Abrudan, I.V. Review of forest ecosystem services evaluation studies in East Africa. *Front. Ecol. Evol.* **2024**, *12*, 1385351. https://doi.org/10.3389/fevo.2024.1385351.
3. Wang, X.; Wang, B.; Cui, F. Exploring ecosystem services interactions in the dryland: Socio-ecological drivers and thresholds for better ecosystem management. *Ecol. Indic.* **2024**, *159*, 111699. https://doi.org/10.1016/j.ecolind.2024.111699.
4. Yasin, E.H.E.; Mulyana, B. Spatial distribution of tree species composition and carbon stock in Tozi tropical dry forest, Sinnar State, Sudan. *Biodiversitas* **2022**, *23*, 230513. https://doi.org/10.13057/biodiv/d230513.
5. Yasin, E.H.E.; Siddig, A.A.H.; Kornel, C. Forests at the crossroads: Biodiversity conservation in the era of climate change. In *Sustainable Forest Management—Surpassing Climate Change and Land Degradation*; Kulshreshtha, S.N., Ed.; IntechOpen: London, UK, 2024. https://doi.org/10.5772/intechopen.1004224.
6. FAO. *Global Forest Resources Assessment 2010*; Food and Agriculture Organization of the United Nations: Rome, Italy, 2010.
7. Price, D.T.; Alfaro, R.I.; Brown, K.J.; Flannigan, M.D.; Fleming, R.A.; Hogg, E.H.; Girardin, M.P.; Lakusta, T.; Johnston, M.; McKenney, D.W. Anticipating the consequences of climate change for Canada's boreal forest ecosystems. *Environ. Rev.* **2013**, *21*, 322–365. https://doi.org/10.1139/er-2013-0042.
8. Gauthier, S.; Bernier, P.; Kuuluvainen, T.; Shvidenko, A.Z.; Schepaschenko, D.G. Boreal forest health and global change. *Science* **2015**, *349*, 819–822. https://doi.org/10.1126/science.aaa9092.
9. Coleine, C.; Delgado-Baquerizo, M.; DiRuggiero, J.; Guirado, E.; Harfouche, A.L.; Perez-Fernandez, C.; Egidi, E. Dryland microbiomes reveal community adaptations to desertification and climate change. *ISME J.* **2024**, *18*, wrae056. https://doi.org/10.1093/ismejo/wrae056.
10. Gurashi, N.A.; Yasin, E.H.E.; Czimber, K. Changes in structure, tree species composition, and diversity of the Abu Geili Riverine Forest Reserve, Sinnar State, Sudan. *Acta Silv. Lign. Hung.* **2024**, *20*, 55–70. https://doi.org/10.37045/aslh-2024-0004.
11. Musa, F.I.; Mohammed, M.H.; Fragallah, S.D.A.; Adam, H.E.; Sahoo, U.K. Current status of tree species diversity at Abu Gadaf Natural Forest Reserve, Blue Nile Region—Sudan. *Vegetos* **2024**, *37*, 1760–1771. https://doi.org/10.1007/s42535-024-00931-2.
12. Sabins, F.F., Jr.; Ellis, J.M. *Remote Sensing: Principles, Interpretation, and Applications*, 4th ed.; Waveland Press: Long Grove, IL, USA, 2020.
13. Abuelbashar, A.I.; Ahmed, D.A.M.D.A.; Siddig, A.A.H.; Yagoub, Y.E.; Gibreel, H.H. Analysis of composition and diversity of natural regeneration of woody species in Jebel El Gerrie dry land forest east of Blue Nile State, Sudan. *J. For. Environ. Sci.* **2022**, *38*, 90–101. https://doi.org/10.7747/JFES.2022.38.2.90
14. Rajasugunasekar, D.; Patel, A.K.; Devi, K.B.; Singh, A.; Selvam, P.; Chandra, A. An integrative review for the role of forests in combating climate change and promoting sustainable development. *Int. J. Environ. Clim. Chang.* **2023**, *13*, 4331–4341. https://doi.org/10.9734/ijecc/2023/v13i113614.
15. Serbouti, S.; Ettaqy, A.; Boukcim, H.; Mderssa, M.E.; El Ghachtouli, N.; Abbas, Y. Forests and woodlands in Morocco: Review of historical evolution, services, priorities for conservation measures and future research. *Int. For. Rev.* **2023**, *25*, 121–145. https://doi.org/10.1505/146554823836838745.
16. Yasin, E.H.E.; Siddig, A.A.H.; Diab, E.E.; Czimber, K. Evaluating the efficiency of two ecological indices in monitoring forest degradation in the drylands of Sudan. *Remote Sens.* **2025**, *17*, 2298. https://doi.org/10.3390/rs17132298.
17. Mohammed, E.M.I.; Hassan, T.T.; Idris, E.A.; Abdel-Magid, T.D. Tree population structure, diversity, regeneration status, and potential disturbances in Abu Gadaf natural reserved forest, Sudan. *Environ. Chall.* **2021**, *5*, 100366. https://doi.org/10.1016/j.envc.2021.100366.
18. Lu, Y.; Zhang, B.; Zhang, M.; Jie, M.; Guo, S.; Wang, Y. Relict plants are better able to adapt to climate change: Evidence from desert shrub communities. *Plants* **2023**, *12*, 4065. https://doi.org/10.3390/plants12234065.

19. Musa, F.I.; Sahoo, U.K. Role of sustainable forest management in poverty reduction and livelihood improvement in Sudan: A review. *Int. J. Ecol. Environ. Sci.* **2023**, *49*, 449–456. https://doi.org/10.55863/ijees.2023.3036.
20. Fassnacht, F.E.; Latifi, H.; Stereńczak, K.; Modzelewska, A.; Lefsky, M.; Waser, L.T.; Straub, C.; Ghosh, A. Review of studies on tree species classification from remotely sensed data. *Remote Sens. Environ.* **2016**, *186*, 64–87. https://doi.org/10.1016/j.rse.2016.08.013.
21. Dalponte, M.; Ørka, H.O.; Gobakken, T.; Gianelle, D.; Næsset, E. Tree species classification in boreal forests with hyperspectral data. *IEEE Trans. Geosci. Remote Sens.* **2013**, *51*, 2632–2645. https://doi.org/10.1109/TGRS.2012.2216272.
22. Smith, W.K.; Dannenberg, M.P.; Yan, D.; Herrmann, S.; Barnes, M.L.; Barron-Gafford, G.A.; Dawson, T.E. Remote sensing of dryland ecosystem structure and function: Progress, challenges, and opportunities. *Remote Sens. Environ.* **2019**, *233*, 111401. https://doi.org/10.1016/j.rse.2019.111401.
23. D'Odorico, P.; Bhattachan, A. Hydrologic variability in dryland regions: Impacts on ecosystem dynamics and food security. *Philos. Trans. R. Soc. B* **2012**, *367*, 3145–3157. https://doi.org/10.1098/rstb.2012.0016.
24. Tucker, C.J. Red and photographic infrared linear combinations for monitoring vegetation. *Remote Sens. Environ.* **1979**, *8*, 127–150. https://doi.org/10.1016/0034-4257(79)90013-0.
25. Huete, A.; Didan, K.; Miura, T.; Rodriguez, E.P.; Gao, X.; Ferreira, L.G. Overview of the radiometric and biophysical performance of the MODIS vegetation indices. *Remote Sens. Environ.* **2002**, *83*, 195–213. https://doi.org/10.1016/S0034-4257(02)00096-2.
26. Persson, M.; Lindberg, E.; Reese, H. Tree species classification with multi-temporal Sentinel-2 data. *Remote Sens.* **2018**, *10*, 1794. https://doi.org/10.3390/rs10111794.
27. Michałowska, M.; Rapiński, J. A review of tree species classification based on airborne LiDAR data and applied classifiers. *Remote Sens.* **2021**, *13*, 353. https://doi.org/10.3390/rs13030353.
28. Zhong, L.; Dai, Z.; Fang, P.; Cao, Y.; Wang, L. Tree species classification based on remote sensing data and classic deep learning-based methods: A review. *Forests* **2024**, *15*, 852. https://doi.org/10.3390/f15050852.
29. Torres, R.; Snoeij, P.; Geudtner, D.; Bibby, D.; Davidson, M.; Attema, E.; Brown, M. GMES Sentinel-1 mission. *Remote Sens. Environ.* **2012**, *120*, 9–24. https://doi.org/10.1016/j.rse.2011.05.028.
30. Drusch, M.; Del Bello, U.; Carlier, S.; Colin, O.; Fernandez, V.; Gascon, F.; Martimort, P. Sentinel-2: ESA's optical high-resolution mission for GMES operational services. *Remote Sens. Environ.* **2012**, *120*, 25–36. https://doi.org/10.1016/j.rse.2011.11.026.
31. Qi, J.; Chehbouni, A.; Huete, A.R.; Kerr, Y.H.; Sorooshian, S. A modified soil adjusted vegetation index. *Remote Sens. Environ.* **1994**, *48*, 119–126. https://doi.org/10.1016/0034-4257(94)90134-1.
32. Farr, T.G.; Rosen, P.A.; Caro, E.; Crippen, R.; Duren, R.; Hensley, S.; Alsdorf, D. The Shuttle Radar Topography Mission. *Rev. Geophys.* **2007**, *45*, RG2004. https://doi.org/10.1029/2005RG000183.
33. Naidoo, R.; Hill, K. Emergence of indigenous vegetation classifications through integration of traditional ecological knowledge and remote sensing analyses. *Environ. Manag.* **2006**, *38*, 377–387. https://doi.org/10.1007/s00267-004-0338-9.
34. Sesnie, S.E.; Gessler, P.E.; Finegan, B.; Thessler, S. Integrating Landsat TM and SRTM-DEM derived variables with decision trees for habitat classification and change detection in complex neotropical environments. *Remote Sens. Environ.* **2008**, *112*, 2145–2159. https://doi.org/10.1016/j.rse.2007.08.025.
35. Hu, B.; Li, Q.; Hall, G.B. A decision-level fusion approach to tree species classification from multi-source remotely sensed data. *ISPRS Open J. Photogramm. Remote Sens.* **2021**, *1*, 100002. https://doi.org/10.1016/j.ophoto.2021.100002.
36. Belgiu, M.; Drăguţ, L. Random Forest in remote sensing: A review of applications and future directions. *ISPRS J. Photogramm. Remote Sens.* **2016**, *114*, 24–31. https://doi.org/10.1016/j.isprsjprs.2016.01.011.
37. De'ath, G.; Fabricius, K.E. Classification and regression trees: A powerful yet simple technique for ecological data analysis. *Ecology* **2000**, *81*, 3178–3192. https://doi.org/10.1890/0012-9658(2000)081[3178:CARTAP]2.0.CO;2.
38. Halldorsson, G.H.; Benediktsson, J.A.; Sveinsson, J.R. Support vector machines in multisource classification. In *Proceedings of the IEEE International Geoscience and Remote Sensing Symposium (IGARSS 2003), Toulouse, France, 21–25 July 2003*; IEEE: Piscataway, NJ, USA, 2003; Volume 3, pp. 2054–2056. https://doi.org/10.1109/IGARSS.2003.1294337.
39. Gorelick, N.; Hancher, M.; Dixon, M.; Ilyushchenko, S.; Thau, D.; Moore, R. Google Earth Engine: Planetary-scale geospatial analysis for everyone. *Remote Sens. Environ.* **2017**, *202*, 18–27. https://doi.org/10.1016/j.rse.2017.06.031.
40. Wang, L.; Diao, C.; Xian, G.; Yin, D.; Lu, Y.; Zou, S.; Erickson, T.A. A summary of the special issue on remote sensing of land change science with Google Earth Engine. *Remote Sens. Environ.* **2020**, *248*, 112002. https://doi.org/10.1016/j.rse.2020.112002.
41. Zhou, L.; Okin, G.S.; Zhang, J. Leveraging Google Earth Engine and machine learning algorithms to incorporate in situ measurement from different times for rangelands monitoring. *Remote Sens. Environ.* **2020**, *236*, 111521. https://doi.org/10.1016/j.rse.2019.111521.

42. Harrison, M.N.; Jackson, J.K. *Ecological Classification of the Vegetation of the Sudan*; Forest Bulletin No. 2; Forest Department, Ministry of Agriculture: Khartoum, Sudan, 1958.
43. Ibrahim, E.M.I.; Osman, E.; Idris, E. Modelling the relationship between crown width and diameter at breast height for naturally grown *Terminalia* tree species. *J. Nat. Resour. Environ. Stud.* **2014**, *6*, 42–49.
44. Ibrahim, E.M.I.; Osman, E.H. Diameter at breast height–crown width prediction models for *Anogeissus leiocarpus* (DC.) Guill. & Perr. and *Combretum hartmannianum* Schweinf. *J. For. Prod. Ind.* **2014**, *3*, 191–197.
45. Gibreel, H.H.; Kordofani, M.A.I.; Warrag, E.I.; Ahmed, H.O. Medicinal value and eco-taxonomy of the flora of Blue Nile State, Sudan. *J. Chem. Pharm. Res.* **2013**, *5*, 36–43.
46. Fahmi, M.K.M. Climate, Trees and Agricultural Practices: Implications for Food Security in the Semi-Arid Zone of Sudan. Ph.D. Thesis, University of Helsinki, Tropical Forestry Department, Helsinki, Finland, 2017.
47. Immitzer, M.; Atzberger, C.; Koukal, T. Tree species classification with Random Forest using very high spatial resolution 8-band WorldView-2 satellite data. *Remote Sens.* **2012**, *4*, 2661–2693. https://doi.org/10.3390/rs4092661.
48. Praticò, S.; Solano, F.; Di Fazio, S.; Modica, G. Machine learning classification of Mediterranean forest habitats in Google Earth Engine based on seasonal Sentinel-2 time-series and input image composition optimisation. *Remote Sens.* **2021**, *13*, 586. https://doi.org/10.3390/rs13040586.
49. Axelsson, A.; Lindberg, E.; Reese, H.; Olsson, H. Tree species classification using Sentinel-2 imagery and Bayesian inference. *Int. J. Appl. Earth Obs. Geoinf.* **2021**, *100*, 102318. https://doi.org/10.1016/j.jag.2021.102318.
50. Abdelrahim, M. Contribution of non-wood forest products in support of livelihoods of rural people living in the area south of Blue Nile State, Sudan. *Int. J. Agric. For. Fish.* **2015**, *3*, 189–194.
51. Abdou, L.; Morou, B.; Abasse, T.; Mahamane, A. Analysis of the structure and diversity of *Prosopis africana* (G. et Perr.) Taub. tree stands in southeastern Niger. *J. Plant Stud.* **2016**, *5*, 58. https://doi.org/10.5539/jps.v5n1p58.
52. Congalton, R.G.; Green, K. *Assessing the Accuracy of Remotely Sensed Data: Principles and Practices*, 3rd ed.; CRC Press: Boca Raton, FL, USA, 2019. https://doi.org/10.1201/9780429052729.
53. Pal, M. Random Forest classifier for remote sensing classification. *Int. J. Remote Sens.* **2005**, *26*, 217–222. https://doi.org/10.1080/01431160412331269698.
54. Breiman, L. Random forests. *Mach. Learn.* **2001**, *45*, 5–32. https://doi.org/10.1023/A:1010933404324.
55. Breiman, L.; Friedman, J.H.; Olshen, R.A.; Stone, C.J. *Classification and Regression Trees*; Routledge: New York, NY, USA, 2017. https://doi.org/10.1201/9781315139470.
56. Cortes, C.; Vapnik, V. Support-vector networks. *Mach. Learn.* **1995**, *20*, 273–297. https://doi.org/10.1007/BF00994018.
57. Ramezan, C.A.; Warner, T.A.; Maxwell, A.E. Evaluation of sampling and cross-validation tuning strategies for regional-scale machine learning classification. *Remote Sens.* **2019**, *11*, 185. https://doi.org/10.3390/rs11020185.
58. Lundberg, S.M.; Lee, S.-I. A unified approach to interpreting model predictions. In Proceedings of the Advances in Neural Information Processing Systems 30, Long Beach, CA, USA, 4–9 December 2017; pp. 5998–6008. Available online: https://proceedings.neurips.cc/paper/2017/hash/8a20a8621978632d76c43dfd28b67767-Abstract.html (accessed on 4 April 2026).
59. James, G.; Witten, D.; Hastie, T.; Tibshirani, R. *An Introduction to Statistical Learning: With Applications in R*; Springer: New York, NY, USA, 2013. https://doi.org/10.1007/978-1-4614-7138-7.
60. Kuhn, M.; Johnson, K. *Applied Predictive Modeling*; Springer: New York, NY, USA, 2013. https://doi.org/10.1007/978-1-4614-6849-3.
61. Chung, L.C.H.; Xie, J.; Ren, C. Improved machine-learning mapping of local climate zones in metropolitan areas using composite Earth observation data in Google Earth Engine. *Build. Environ.* **2021**, *199*, 107879. https://doi.org/10.1016/j.buildenv.2021.107879.
62. Vorpahl, P.; Elsenbeer, H.; Märker, M.; Schröder, B. How can statistical models help to determine driving factors of landslides? *Ecol. Model.* **2012**, *239*, 27–39. https://doi.org/10.1016/j.ecolmodel.2011.12.007.
63. Ließ, M.; Glaser, B.; Huwe, B. Uncertainty in the spatial prediction of soil texture: Comparison of regression tree and random forest models. *Geoderma* **2012**, *170*, 70–79. https://doi.org/10.1016/j.geoderma.2011.10.010.
64. Bishop, C.M.; Nasrabadi, N.M. *Pattern Recognition and Machine Learning*; Springer: New York, NY, USA, 2006.
65. Ali, Y.A.; Awwad, E.M.; Al-Razgan, M.; Maarouf, A. Hyperparameter search for machine learning algorithms for optimizing the computational complexity. *Processes* **2023**, *11*, 349. https://doi.org/10.3390/pr11020349.
66. Strömann, O.; Nascetti, A.; Yousif, O.; Ban, Y. Dimensionality reduction and feature selection for object-based land cover classification based on Sentinel-1 and Sentinel-2 time series using Google Earth Engine. *Remote Sens.* **2020**, *12*, 76. https://doi.org/10.3390/rs12010076.

67. Fathizad, H.; Ardakani, M.A.H.; Sodaiezadeh, H.; Kerry, R.; Taghizadeh-Mehrjardi, R. Investigation of the spatial and temporal variation of soil salinity using random forests in the central desert of Iran. *Geoderma* **2020**, *365*, 114233. https://doi.org/10.1016/j.geoderma.2020.114233.
68. Lu, D.; Weng, Q. A survey of image classification methods and techniques for improving classification performance. *Int. J. Remote Sens.* **2007**, *28*, 823–870. https://doi.org/10.1080/01431160600746456.
69. Lee, J.S.H.; Wich, S.; Widayati, A.; Koh, L.P. Detecting industrial oil palm plantations on Landsat images with Google Earth Engine. *Remote Sens. Appl. Soc. Environ.* **2016**, *4*, 219–224. https://doi.org/10.1016/j.rsase.2016.11.003.
70. Olofsson, P.; Foody, G.M.; Herold, M.; Stehman, S.V.; Woodcock, C.E.; Wulder, M.A. Good practices for estimating area and assessing accuracy of land change. *Remote Sens. Environ.* **2014**, *148*, 42–57. https://doi.org/10.1016/j.rse.2014.02.015.
71. FAO. *Map Accuracy Assessment and Area Estimation: A Practical Guide*; FAO Forestry Paper 185; FAO: Rome, Italy, 2016. Available online: https://openknowledge.fao.org/handle/20.500.14283/I5601E (accessed on 4 April 2026).
72. Stehman, S.V. Estimating area and map accuracy for stratified random sampling when the strata are different from the map classes. *Remote Sens. Environ.* **2014**, *139*, 137–146. https://doi.org/10.1080/01431161.2014.930207.
73. Raczko, E.; Zagajewski, B. Comparison of support vector machine, random forest and neural network classifiers for tree species classification on airborne hyperspectral APEX images. *Eur. J. Remote Sens.* **2017**, *50*, 144–154. https://doi.org/10.1080/22797254.2017.1299557
74. Sabat-Tomala, A.; Raczko, E.; Zagajewski, B. Comparison of support vector machine and random forest algorithms for invasive and expansive species classification using airborne hyperspectral data. *Remote Sens.* **2020**, *12*, 516. https://doi.org/10.3390/rs12030516.
75. Karlson, M.; Reese, H.; Ostwald, M. Tree crown mapping in managed woodlands (parklands) of semi-arid West Africa using WorldView-2 imagery and geographic object-based image analysis. *Sensors* **2014**, *14*, 22643–22669. https://doi.org/10.3390/s141222643.
76. Wan, H.; Tang, Y.; Jing, L.; Li, H.; Qiu, F.; Wu, W. Tree species classification of forest stands using multisource remote sensing data. *Remote Sens.* **2021**, *13*, 144. https://doi.org/10.3390/rs13010144.
77. Soleimannejad, L.; Ullah, S.; Abedi, R.; Dees, M.; Koch, B. Evaluating the potential of Sentinel-2, Landsat-8, and IRS satellite images in tree species classification of Hyrcanian forests using random forest. *J. Sustain. For.* **2019**, *38*, 615–628. https://doi.org/10.1080/10549811.2019.1598443.
78. Ferreira, M.P.; Wagner, F.H.; Aragão, L.E.O.C.; Shimabukuro, Y.E.; de Souza Filho, C.R. Tree species classification in tropical forests using visible to shortwave infrared WorldView-3 images and texture analysis. *ISPRS J. Photogramm. Remote Sens.* **2019**, *149*, 119–131. https://doi.org/10.1016/j.isprsjprs.2019.01.019.
79. Du, P.; Samat, A.; Waske, B.; Liu, S.; Li, Z. Random forest and rotation forest for fully polarized SAR image classification using polarimetric and spatial features. *ISPRS J. Photogramm. Remote Sens.* **2015**, *105*, 38–53. https://doi.org/10.1016/j.isprsjprs.2015.03.002.
80. Wang, H.; Magagi, R.; Goïta, K.; Trudel, M.; McNairn, H.; Powers, J. Crop phenology retrieval via polarimetric SAR decomposition and random forest algorithm. *Remote Sens. Environ.* **2019**, *231*, 111234. https://doi.org/10.1016/j.rse.2019.111234.
81. Xu, Z.; Shen, X.; Cao, L.; Coops, N.C.; Goodbody, T.R.; Zhong, T.; Wu, X. Tree species classification using UAS-based digital aerial photogrammetry point clouds and multispectral imageries in subtropical natural forests. *Int. J. Appl. Earth Obs. Geoinf.* **2020**, *92*, 102173. https://doi.org/10.1016/j.jag.2020.102173.
82. Liu, M.; Liu, J.; Atzberger, C.; Jiang, Y.; Ma, M.; Wang, X. *Zanthoxylum bungeanum* Maxim mapping with multi-temporal Sentinel-2 images: The importance of different features and consistency of results. *ISPRS J. Photogramm. Remote Sens.* **2021**, *174*, 68–86. https://doi.org/10.1016/j.isprsjprs.2021.02.003.
83. Bahrami, H.; Chokmani, K.; Homayouni, S.; Adamchuk, V.I.; Saifuzzaman, M.; Albasha, R.; Leduc, M. Alfalfa stem count estimation using remote sensing imagery and machine learning on Google Earth Engine. *Int. J. Appl. Earth Obs. Geoinf.* **2025**, 142, 104729. https://doi.org/10.1016/j.jag.2025.104729.

Disclaimer/Publisher's Note: The statements, opinions and data contained in all publications are solely those of the individual author(s) and contributor(s) and not of MDPI and/or the editor(s). MDPI and/or the editor(s) disclaim responsibility for any injury to people or property resulting from any ideas, methods, instructions or products referred to in the content.